The Soil Moisture Active Passive Experiments (SMAPEx): Toward Soil Moisture Retrieval From the SMAP Mission

Rocco Panciera, Jeffrey P. Walker, Thomas J. Jackson, *Fellow, IEEE*, Douglas A. Gray, Mihai A. Tanase, Dongryeol Ryu, Alessandra Monerris, Heath Yardley, Christoph Rüdiger, *Member, IEEE*, Xiaoling Wu, Ying Gao, and Jörg M. Hacker

***Abstract*—NASA's Soil Moisture Active Passive (SMAP) mission will carry the first combined spaceborne L-band radiometer and Synthetic Aperture Radar (SAR) system with the objective of mapping near-surface soil moisture and freeze/thaw state globally every 2–3 days. SMAP will provide three soil moisture products: i) high-resolution from radar (∼3 km), ii) low-resolution from radiometer (∼36 km), and iii) intermediate-resolution from the fusion of radar and radiometer (∼9 km). The Soil Moisture Active Passive Experiments (SMAPEx) are a series of three airborne field experiments designed to provide prototype SMAP data for the development and validation of soil moisture retrieval algorithms applicable to the SMAP mission. This paper describes the SMAPEx sampling strategy and presents an overview of the data collected during the three experiments: SMAPEx-1 (July 5–10, 2010), SMAPEx-2 (December 4–8, 2010) and SMAPEx-3 (September 5–23, 2011). The SMAPEx experiments were conducted in a semi-arid agricultural and grazing area located in southeastern Australia, timed so as to acquire data over a seasonal cycle at various stages of the crop growth. Airborne L-band brightness temperature (∼1 km) and radar backscatter (∼10 m) observations were collected over an area the size of a single SMAP footprint (38 km × 36 km at 35° latitude) with a 2–3 days revisit time, providing SMAP-like data for testing of radiometer-only, radar-only and combined radiometer-radar soil moisture retrieval and downscaling algorithms. Airborne observations were supported by continuous monitoring of near-surface (0–5 cm) soil moisture along with intensive ground monitoring of soil moisture, soil temperature, vegetation biomass and structure, and surface roughness.**

Manuscript received May 22, 2012; revised November 22, 2012; accepted January 1, 2013. The SMAPEx experiments were funded by an Australian Research Council Discovery Project (DP0984586).

R. Panciera and M. A. Tanase are with the Cooperative Research Center for Spatial Information, The University of Melbourne, Melbourne, Vic. 3053, Australia (e-mail: panr@unimelb.edu.au; mihai76@gmail.com).

J. P. Walker, A. Monerris, C. Rüdiger, X. Wu, and Y. Gao are with the Department of Civil Engineering, Monash University, Victoria 3800, Australia (e-mail: jeff.walker@monash.edu; sandra.monerris-belda@monash.edu; chris.rudiger@monash.edu; xiaoling.wu@monash.edu; ying.gao@monash.edu).

T. J. Jackson is with USDA-ARS Hydrology and Remote Sensing Lab, Beltsville, MD 20705 USA (e-mail: tom.jackson@ars.usda.gov).

D. A. Gray and H. Yardley are with the Radar Research Centre, EEE School, The University of Adelaide, Adelaide, SA 5005, Australia (e-mail: dgray@eleceng.adelaide.edu.au; Heath.Yardley@dsto.defence.gov.au.adelaide.edu.au).

D. Ryu is with the Melbourne School of Engineering, The University of Melbourne, Melbourne, Vic. 3053, Australia (e-mail: ryu.dongryeol@gmail.com).

J. M. Hacker is with the Airborne Research Australia, Flinders University, Salisbury South, SA 5106, Australia (e-mail: jorg@airborneresearch.com.au).

Color versions of one or more of the figures in this paper are available online at http://ieeexplore.ieee.org.

Digital Object Identifier 10.1109/TGRS.2013.2241774

***Index Terms*—L-band, microwave, polarimetric L-band imaging synthetic aperture radar (PLIS), polarimetric L-band multibeam radiometer (PLMR), remote sensing, soil moisture active passive (SMAP), soil moisture, synthetic aperture radar (SAR).**

I. Introduction

THE Soil Moisture Active Passive (SMAP) satellite will use combined passive (radiometer) and active (radar) microwave instruments at L-band to measure the land hydrospheric state globally [1]. SMAP will provide measurements of near-surface soil moisture (0–5 cm depth) and land freeze/thaw condition over a 1000 km swath with a global revisit of 2–3 days. Soil moisture is a crucial land surface state variable that controls the land-atmosphere interactions [2]–[4]. Consequently, the SMAP measurements are expected to make significant contributions to weather and climate forecasting skills including the prediction of extreme hydrological events such as droughts and floods, thus impacting on agricultural productivity and human health [1].

Global soil moisture observations have been available from passive microwave sensors such as the C/X-band (∼6/10 GHz) Advanced Microwave Scanning Radiometer (AMSR-E, ceased operations but replaced by AMSR2 in May 2012) as well as active microwave sensors like the C-band Advanced Synthetic Aperture Radar (ASAR, ceased operations in 2011). Although a soil moisture product is also available from the C-band Advanced SCAT terometer (ASCAT) [5], C-band observations are not optimal for soil moisture retrieval as they are sensitive to a shallower soil layer than L-band observations and are more significantly affected by vegetation attenuation [6]. Currently the only soil moisture dedicated satellite is the L-band (∼1.4 GHz) Soil Moisture and Ocean Salinity (SMOS) mission [7].

The synthetic aperture L-band radiometer of SMOS has optimum sensitivity to soil moisture but low spatial resolution (approximately 40 km), which poses a limitation for its use in hydrometeorological and agricultural applications requiring soil moisture information at resolutions of 10 km or higher [8], [9]. Active sensors, while having the capability to provide higher spatial resolution, present the added complication of being sensitive to the geometric structure of the soil surface and the vegetation layer, whose scattering and absorption mechanism are still an elusive modeling problem [10]. Consequently, there is currently no spaceborne platform capable of providing

soil moisture data at 10 km spatial resolution with 2–3 day temporal repeat.

The innovative measurement approach of SMAP is to integrate a L-band radar and an L-band radiometer as a single observation system combining the relative strengths of active and passive remote sensing for enhanced soil moisture mapping. The radar observations provide high-resolution but noisy information on soil moisture, which can be combined with the more direct but low-resolution soil moisture information provided by the radiometer. SMAP will therefore enable global soil moisture mapping with unprecedented resolution. Because the effects of vegetation and surface roughness are dependent on incidence angle, and to maximize the independent information obtainable from the radiometer's vertically (V) and horizontally (H) polarized brightness temperature, a rotational scanning configuration with a single incidence angle of 40° has been adopted for SMAP [1]. The wide swath that results from this approach enables SMAP observations to provide global coverage in two to three days.

SMAP will provide three soil moisture products: i) high-resolution radar-only (∼3 km), ii) low-resolution (∼36 km) radiometer-only, and iii) intermediate-resolution combined radar–radiometer (∼9 km). Algorithms for radiometer-only soil moisture retrieval have been developed over an extensive number of field experiments using ground-based instruments in the 1980s [11], [12] and airborne radiometers in numerous field campaigns such as Washita'92 and Southern Great Plains (SGP) '97 and '99 [13]–[15], the series of Soil Moisture Experiments, SMEX [16] and the National Airborne Field Experiments, NAFE [17], [18]. SMAP will therefore take full advantage of this algorithm development heritage, which provides a robust description of the vegetation and surface roughness effects on soil moisture retrievals. Conversely, algorithms for radar-only soil moisture retrieval have not reached the same level of maturity, and there has been little effort on active–passive downscaling.

An intensive period of ground-based radar research undertaken in the 1970s and 1980s established the theoretical basis of soil and vegetation effects on radar backscatter [19]–[21]. However, there have been only few global radar-based applications for soil moisture retrieval, despite the availability of L-band Synthetic Aperture Radar (SAR) data from sensors such as the Japanese Earth Resources Satellite 1 (JERS-1) and the Phased Array type L-band Synthetic Aperture Radar (PALSAR). This is mainly because of the difficulty to account for surface roughness and vegetation in such a way that the models could be applied at global scale [10]. Although detailed analytical scattering models have been developed [21]–[23], the computational burden and level of ancillary data required have hindered global application. Consequently, the most promising approaches rely on empirical or semi-empirical models which approximate the scattering in the vegetation layer in a simplified way. However, such models make use of parameters which are specific to each vegetation type, and therefore require extensive validation [24]–[28].

As a result of the issues discussed above, one of the most pressing research questions to be addressed before the SMAP launch is the development and field testing of techniques to fuse the radar and radiometer measurements to obtain a combined soil moisture product at intermediate resolution. A few studies have analyzed the synergy between radar and radiometer observations using data from the passive and active L- and S-band Sensor (PALS) and the NASA/JPL Airborne SAR (AIRSAR) during SGP'99, SMEX'02 and the Cloud Land Atmospheric Interaction Campaign (CLASIC) 2007 [14], [29], [30]. While these studies did not cover an area comparable to a SMAP footprint, they have provided insights into the potential synergies between the two sensors, and a few techniques have been proposed for merging active and passive data. However, these techniques currently lack evaluation using real data at the scale and resolutions of SMAP observations [31]–[33]. Moreover, the imminent availability of 2–3 day time-series radar observations from SMAP has boosted the interest in using change detection and time series techniques to derive soil moisture estimates from the radar data directly [34]–[36], but such techniques have not been thoroughly tested, due to the lack of exact orbit repeat data providing multi-temporal L-band radar acquisitions at suitable time intervals. More recently, international field experiments aimed at collecting active and passive microwave data for pre-launch assessment of the SMAP soil moisture products included the SMAP Validation EXperiment (SMAPVEX) 2008 [37], [38] and the Canadian Experiment for Soil Moisture in 2010 (CanEX-SM10, [39]). Each of these is a valuable source of data to address specific aspects of the SMAP mission.

The Soil Moisture Active Passive Experiments (SMAPEx) described in this paper complement these international efforts by adopting a monitoring strategy specifically tailored to the spatial and temporal resolutions of the future SMAP products, and by providing data at various stages of a seasonal cycle. The SMAPEx Experiments were designed to provide an extensive data set of L-band radar and radiometer observations to serve as an algorithm development test-bed for the SMAP mission. Thus, airborne observations and supporting ground data were collected over an area the size of a SMAP footprint with 2–3 days revisit time, to simulate the observations expected from SMAP. The experiments were timed to cover various climatic conditions as well as various stages of the crop growing season, including winter onset (SMAPEx-1, July 2010), spring growth (SMAPEx-3, September 2011) and summer senescence (SMAPEx-2, December 2010). While the 1-week long SMAPEx-1 and -2 provided data that support snapshot algorithm developments, the 3-week long SMAPEx-3 focused on providing time-series data sets suitable for change detection and time series algorithm development. The SMAPEx data set therefore represents an important contribution to the development of the SMAP mission. The first part of this paper describes in detail the SMAPEx study area and airborne and ground sampling strategies, and provides an overview of the data collected. An assessment of the quality of the active and passive microwave data and their sensitivity to surface conditions is then presented in light of their potential for soil moisture retrieval.

II. Study Area Description

The SMAPEx study site is a semi-arid agricultural and grazing area located in the western plains of the Murrumbidgee

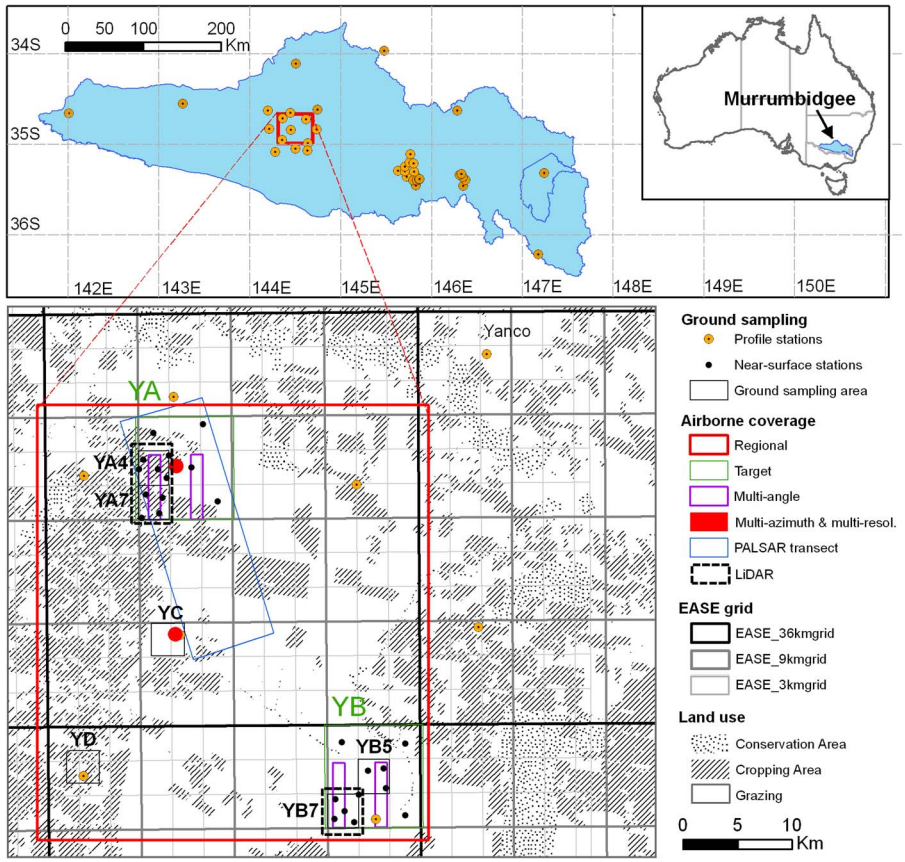

Fig. 1. Bottom panel: Layout of the SMAPEx study area (red rectangle) indicating SMAP EASE grid overlain with airborne and ground monitoring locations. Top panel: Location of the SMAPEx study area (red rectangle) within the murrumbidgee catchment. Inset: Location of the Murrumbidgee catchment within Australia.

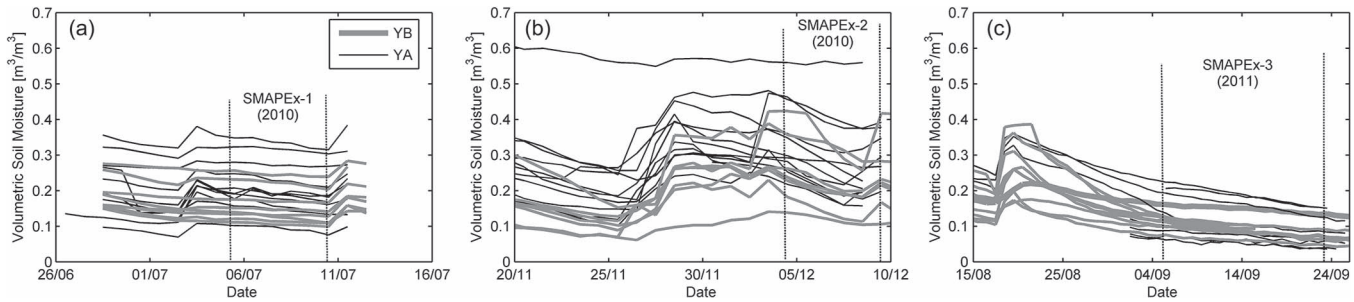

Fig. 2. Daily soil moisture time-series at the SMAPEx near-surface (0–5 cm) monitoring stations for (a) SMAPEx-1, (b) SMAPEx-2, and (c) SMAPEx-3. Different lines represent different monitoring stations across the SMAPEx study area, grouped by target areas (YA, thin black lines or YB, thick gray lines).

catchment near the township of Yanco (see Fig. 1). The area has been monitored for remote sensing research since 2003 with 13 OzNet profile stations measuring soil moisture at various depths (down to 90 cm), upgraded in 2010 with 24 near-surface (0–5 cm) monitoring stations [40] (see www.oznet.org.au). Approximately one third of the Yanco area is occupied by the Coleambally Irrigation Area (CIA), an agricultural area that contains more than 500 farms and is characterized by a dense network of irrigation channels. The principal summer crops grown in the CIA are rice, corn, and soybeans, whereas winter crops include wheat, barley, oats, and canola. In November, rice crops are usually inundated with about 30 cm of irrigation water. The topography of the study area is flat with elevation ranging from 117 to 150 m. The area has already been the focus of other airborne campaigns dedicated to algorithm development studies for the SMOS mission: the National Airborne Field Experiment 2006 (NAFE'06, [18]), and the Australian Airborne Cal/val Experiments for SMOS (AACES, [41]).

III. Overview of Experiments

SMAPEx was comprised of three field experiments conducted in the Yanco study area. SMAPEx-1 was conducted in the austral winter from 5–10 July, 2010 and was characterized by wet winter conditions with soil moisture in the range 0.1–0.4 m^3/m^3 [see Fig. 2(a)]. Moderate rainfall on July 1 (3 mm) followed by a period of little rainfall allowed observation of a dry-down period of approximately 0.05 m^3/m^3 (average decrease across the monitoring stations during the field experiment). There was minimal vegetation cover during

the campaign since the experiment was conducted shortly after planting, with only emergent crops present in the fields. The vegetation water content (VWC) in crop and grass areas was within the range of 0–0.8 kg/m^2. SMAPEx-2 was conducted in the austral summer from 4–8 December 2010. Extreme rainfall was experienced in the study area in the month preceding the experiment, producing unusually wet soil moisture conditions (0.1–0.6 m^3/m^3) for that time of year. With no rainfall experienced during the experiment, a dry-down event was observed yielding a dynamic range of 0.05 to 0.10 m^3/m^3 for most sites, although some sites showed a drop of $\sim$0.15 m^3/m^3 in soil moisture conditions [Fig. 2(b)]. However, the extreme rainfall had produced extensive ponding of surface water in some parts of the study area, which impacted the ground sampling strategy. Due to warm moist conditions and delayed harvests, vegetation biomass was high, with crops at peak or near-peak biomass (VWC up to 4 kg/m^2) and lush native pastures (up to 2.2 kg/m^2). The 3-week long SMAPEx-3 took place in the austral spring between September 5 and 23, 2011. Moderate rainfall in the first half of the sampling period ($\sim$5 mm between September 5–7 and $\sim$3 mm on September 10–12 across the study area), followed by a dry down period, resulted in drier soil moisture conditions than those experienced in the previous experiments (0.05–0.4 m^3/m^3), and a limited dynamic range of only 0.05 m^3/m^3 during the field experiment [Fig. 2(c)]. The SMAPEX-3 experiment was timed to capture a phase of intensive growth of winter crops in the study area (essentially wheat, barley and canola). The increase in plant height was moderate, approximately from 45 to 50 cm for wheat, from 28 to 33 cm for barley, and from 114 to 136 cm for canola (increase calculated as the difference between the average height across all the fields sampled). VWC increased for wheat and canola, from 0.9 to 1.4 kg/m and from 3.9 to 6.6 kg/m^2, respectively, whereas barley was stable at 0.9 kg/m^2. Elevated spatial variability of near-surface soil moisture was observed across the study area in all three experiments, as highlighted in Fig. 2. Wetter conditions and higher spatial variability were observed in the target area "YA", located within the CIA irrigation district (see Fig. 1). This area presented a mix of flood irrigated and dryland cropping areas and grazing areas resulting in highly variable near-surface soil moisture conditions. Conversely, the "YB" target area located in the southern part of the study area, a flat region characterized by uniform grasslands, presented drier and more uniform conditions. This is consistent between campaigns and is reflected in the soil moisture time series presented in Fig. 2.

The SMAPEx airborne and ground monitoring strategy was designed based on the Equal-Area Scalable Earth (EASE) grids on which the SMAP geophysical products will be provided (nsidc.org/data/ease/, Fig. 1). The "Regional" flights covered an area equivalent in size to a single pixel of the nominal 36 km grid of the SMAP Level 2 Soil Moisture Passive product (L2/3_SM_P) and were the primary scientific flights of SMAPEx. Additional "Target" flights focused on two target areas, YA and YB. These corresponded to two nominal 9 km $\times$ 9 km pixels of the Active/Passive product (L2/3_SM_A/P) (Fig. 1), and were selected to be representative of the intensive irrigated and uniform grazing areas in the study site. Spatial ground sampling of soil moisture, soil temperature, vegetation characteristics and surface roughness was undertaken at six focus areas, each matching a radar-sized pixel of the Active-only product (L2/3_SM_A), which were covered on rotation during the experiments. Spatial sampling was complemented by the permanent soil moisture monitoring network, which was also designed based on the multi-resolution grid of SMAP. While providing full coverage of the 36 km pixel, the network presented clusters of sites in the two Target areas YA and YB ($\sim$13 sites each), with 4–5 sites further concentrated in two of the 3 km $\times$ 3 km focus areas in both YA and YB. This configuration provided permanent monitoring at all resolutions relevant to SMAP products (see Fig. 1). Due to variations in EASE grid size according to latitude, in the SMAPEx study area the nominal 36 km and 9 km pixels corresponded to 38 km $\times$ 36 km and 9.5 km $\times$ 8.5 km areas, respectively, whereas for the 3 km pixels the distortion was negligible.

SMAPEx airborne and ground observations were conducted every day for 5 days during SMAPEx-1 and -2. Regional flights were conducted every other day (i.e., first, third, and fifth) with Target flights undertaken in the intervening days. Target flight days were also dedicated to special flights for multi-angle, multi-azimuth, multi-resolution and PALSAR comparison purposes. During SMAPEx-3 a sampling cycle of five consecutive days was repeated across three consecutive weeks, with slight modifications due to unexpected weather changes and to accommodate concurrence with SMOS overpasses, meaning that Regional flights were undertaken with a 1–3 days revisit time. A summary of the flights undertaken during the SMAPEx campaigns is presented in Table I. Spatial ground sampling of soil moisture, vegetation biomass and surface roughness was undertaken concurrently with flights at the focus areas throughout each of the campaigns.

No Target flights were conducted during SMAPEx-3. However, intensive ground sampling of crop geometric properties for modeling of radar scattering, additional vegetation biomass sampling, and extensive surface roughness characterization took place on these intervening days. Moreover, ancillary airborne Light Detection and Ranging (LiDAR) and hyperspectral data were collected over two focus areas (agricultural and grazing) at the start and end of the SMAPEx-3 campaign, to monitor vegetation growth across the experiment period. A specific low altitude LiDAR flight was also undertaken to monitor surface roughness over a few bare soil fields which presented a range of roughness conditions.

IV. Data Description

A. AirBorne Data

1) AirBorne Instruments: The airborne SMAP simulator that is core to the SMAPEx experiments consists of the Polarimetric L-band Multibeam Radiometer (PLMR), installed in push-broom configuration, coupled with the Polarimetric L-band Imaging Synthetic aperture radar (PLIS), in side-looking configuration on both sides of the aircraft. Supporting instrumentation included visible, infrared, near-infrared, short-wave infrared and thermal radiometers. This configuration

TABLE I
SUMMARY OF FLIGHTS. (P) INDICATES THE GROUND RESOLUTION FOR THE PLMR, THERMAL INFRARED AND MULTI-SPECTRAL RADIOMETERS, (Pl) = GROUND RESOLUTION FOR PLIS

Flight type	Coverage	Altitude	Ground Resolution	Dates SMAPEx-1	Dates SMAPEx-2	Dates SMAPEx-3
Regional	Yanco area (38 km x 36km)	3,000m	1 km (P)/ 11-29m (Pl)	Jul 6, 8, 10	Dec 4, 6, 8	Sept 5,7,10,13,15, 18,19,21,23
Target	YA and YB (9 km × 9km)	300m	100m (P)/ 11-29m (Pl)	Jul 7 (YB) Jul 9 (YA)	Dec 5 (YA)	-
Multi-angle	YA & YB (1 km × 6km)	3,000m	1 km (P)/ 11-29m (Pl)	Jul 6, 8, 10	Dec 7(YA)	-
Multi-azimuth	2 areas (1 km × 1km)	1,500m	500m (P)/ 11-29m 29m (Pl)	-	Dec 7	-
Multi-resolution	2 areas (1 km × 1km)	1,500m		-	Dec 7	-
PALSAR transect	8 km × 22km	3,000m	No PLMR/11-29m (Pl)	Jul 5	Dec 7 *(PALSAR observation not acquired)*	*(PALSAR not operational)*
LiDAR, vegetation growth monitoring	3 focus areas (3 km × 3 km ea.)	400m	8pts/m^2	-	-	Sept 5, 22
Hyperspectral, vegetation properties	3 focus areas (3 km × 3 km ea.)	400m	0.8m			Sept 5, 22
LiDAR , surface roughness monitoring	75m × 3km	100m	32pts/m^2 (LiDAR)			Sept 5, 22

allowed imaging surface microwave backscatter at resolution of 11–29 m, and microwave emission, land surface skin temperature and spectral data at 1 km resolution over a 4000 m ground swath with a single pass at 3000 m altitude.

The PLIS is an airborne synthetic aperture digital radar with polarimetric and interferometric capabilities. It radiates pulses at a carrier frequency of 1.26 GHz with a typical bandwidth of 30 MHz in H and V polarization and receives H and V polarizations. PLIS illuminates the ground swaths on either side of the aircraft with an incidence angle varying from 15° to 45° across the swath. For the 30 MHz bandwidth, the PLIS single-look slant range resolution is 6 m, resulting in a ground range resolution varying between 23–8 m (from 15°–45°). The single-look azimuth resolution is 0.8 m. The minimum detectable Normalized Radar Cross Section is -35 dB$/(\mathrm{m}^2/\mathrm{m}^2)$ from 3000 m altitude. More details on the PLIS system can be found in Gray *et al.* [42]. The PLMR is composed of an 8×8 patch array that uses electronic beam forming to produce six pushbroom receivers with across track incidence angles of $\pm 7°$, $\pm 21.5°$, and $\pm 38.5°$. PLMR measures both V and H polarized 1.413 GHz brightness temperatures using a polarization switch. In pushbroom configuration the 3 dB beamwidth is 17° along track and 14° across track resulting in a footprint size of approximately 1 km from 3000 m altitude.

Other airborne instruments onboard the aircraft included six thermal infrared radiometers (8.0–14.0 nm) and 6 multispectral sensors (Skye Instruments Ltd.) that match MODIS bands 1 (620–670 nm), 2 (841–876 nm), 3 (459–479 nm), 4 (545–565 nm), 6 (1628–1652 nm) and 7 (2105–2155 nm), plus 2 additional short-wave infrared bands at 2026–2036 nm and 2206–2216 nm. All sensors have a 15° beamwidth closely matching that of PLMR (14°–17°), and were installed at the same incidence angles as the PLMR beams to give coincident microwave, visible, infrared and thermal infrared footprints. The set up was complemented by a Canon EOS-1Ds Mark III that provides 21 MegaPixel aerial images.

The LiDAR and hyperspectral observations for vegetation and surface roughness monitoring during SMAPEx-3 were collected using a second aircraft operated by Airborne Research Australia. Instruments onboard this aircraft included a RIEGL LMS-Q560 2-D full-waveform laser scanner and the Short Wave Infrared (970–2500 nm) hyperspectral "Hawk," with additional Tri-Spectral (G,R,NIR) and single channel (950 nm) line scanners.

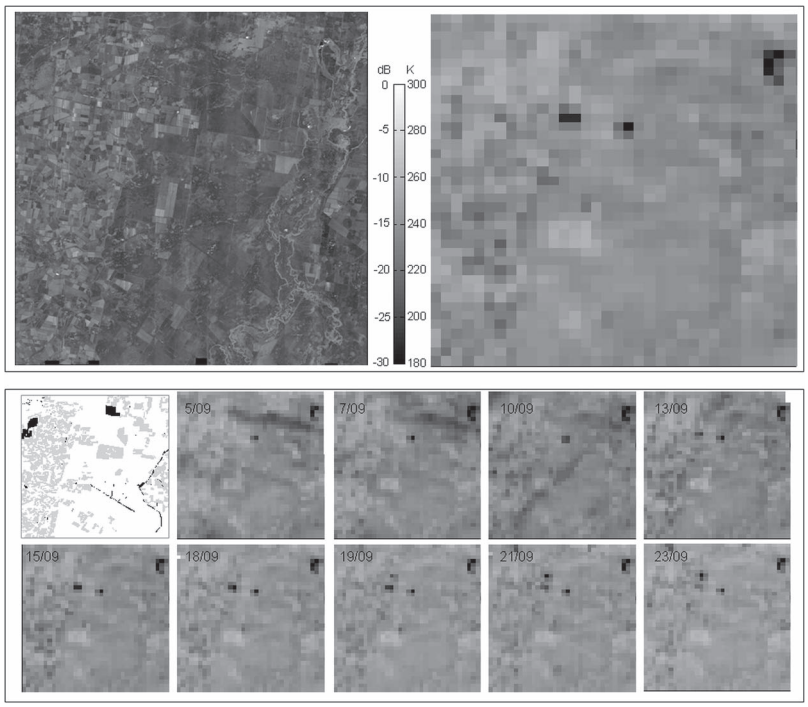

Fig. 3. Example of Regional radar and radiometer coverage of the SMAPEx study area (38 km × 36 km). Top panel: Comparison of radar backscatter at HH-polarization and 10 m resolution (left) with concurrent radiometer brightness temperatures at H-pol and 1 km resolution (right). Bottom panel: Time series of 1 km H-pol radiometer coverage (September 5–23). The landcover map of the study area is also provided to aid interpretation (white = grazing, gray = crops, black = woodland). All observations are normalized to 40° incidence angle.

2) Regional Flights: Regional flights were the core activity of the SMAPEx campaigns, with the objective of providing prototype SMAP data for development and testing of techniques for joint active and passive soil moisture retrieval and downscaling. The 1 km brightness temperature together with 11–29 m resolution backscatter observations were mapped over an area that matched the size of a SMAP radiometer footprint (38 km × 36 km). The entire area was covered in just over 2 hours of flying at 3000 m altitude using north–south oriented flight lines. A partial repeat of the first flight line was performed to assess temporal changes in brightness temperature during mapping. Regional flights were repeated with a temporal frequency consistent with the planned SMAP revisit time of 2–3 days. Fig. 3 presents a sample of the concurrent radar and radiometer acquisitions during SMAPEx-3. Both radar and radiometer acquisitions are sensitive to ground features, in particular the distinction between irrigated crops, pasture and woodland. The brightness temperature gradients between the North-West and South-East portion of the study area are consistent with the ground observations presented in Fig. 2, showing wetter soil moisture conditions in the irrigation district YA as opposed to the grazing land in YB. The radiometer time series exhibit a gradual dry-down over the experiment period and also reflect the sporadic moist conditions associated with the rainfall events in the north-eastern part of the study area on September 5 and 7.

3) Target Flights: On each Target day, one of the two Target areas YA and YB was mapped using north–south oriented flight lines from a 300 m altitude. Given that the PLIS ground resolution is invariant with altitude, this provided radiometer data with a ground resolution comparable to that of the radar (100 m radiometer and 11–29 m radar) for detailed comparison of active and passive microwave land signature, and development of joint active and passive soil moisture retrieval techniques. During SMAPEx-2, Target flights were restricted to the YA area only due to extensive flooding affecting the YB area. No Target flights were undertaken during SMAPEx-3 as this was not part of the objective for that campaign. Fig. 4 presents an example of the high-resolution airborne radiometer and spectral measurement observations during Target flights. Despite some evidence of incidence angle effects not yet properly corrected for at this stage (visible in the north–south striping), the high-resolution images clearly display the changing radiometric signature captured in an area characterized by a strong contrast between irrigated cropping and dry land pasture across the 2010 growing season (SMAPEx-1 and 2).

4) Multi-Angle Flights: The radar backscatter of a surface is known to be dependent on the angle formed by the incident wave with the surface. This angle can be characterized using the incidence view angle (the angle formed on a vertical plane between the incident wave and the nadir direction) and the azimuth view angle (the angle formed on a horizontal plane between the incident wave and a reference direction). Multi-angle flights were designed to provide radar observations of the same ground locations at a variety of incidence view angles, with the two-fold objective of providing data for i) developing incidence angle normalization techniques so that SMAP-like data at constant 40° incidence angle can be simulated and ii) characterize the angular signature of various crop types for radar backscatter algorithm development. Two focus ground strips (1 km × 6 km) were mapped in Target areas YA and YB, with each strip representative of irrigated cropping and grazing land

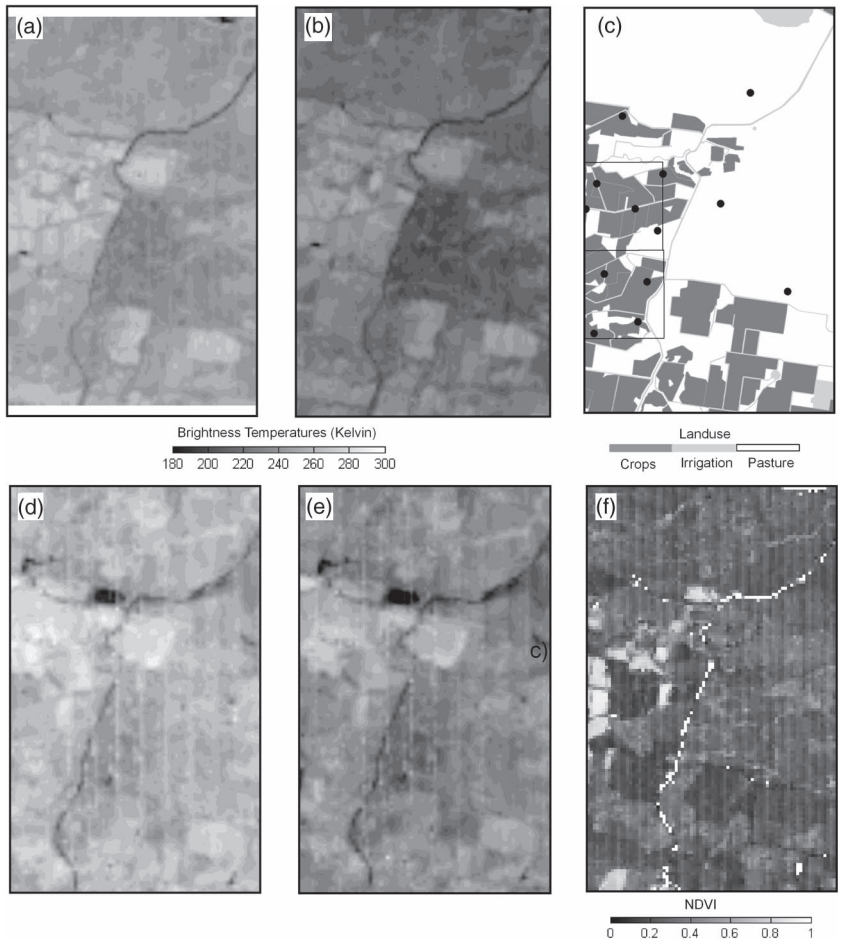

Fig. 4. Example of airborne coverage of the SMAPEx Target area YA (9 km × 3 km): Radiometer brightness temperatures at 100 m resolution for V-pol (left) and H-pol (right) at the onset of the crop growing season, July 9 (a), (b) and at crop maturity, December 5 (d), (e). All observations are normalized to 40° incidence angle. Additionally shown are (c) a land use map of the area (with ground sampling areas as black rectangles and near-surface monitoring stations as black dots), and (f) airborne NDVI at 100 m resolution collected concurrently with radiometer observations on December 5. The north–south striping visible in the December brightness temperatures and NDVI data is due to incidence angle effects not yet properly corrected for at this stage.

respectively (Fig. 1). The 360 m-spaced flight lines at 3000 m altitude provided radar backscatter at incidence angles spanning the PLIS beamwidth (15°–45°) with a 5° step. The majority of the multi-angle flights were undertaken during SMAPEx-1 in conjunction with the Regional flights. During SMAPEx-2 only one multi-angle flight was performed to check for the change in backscatter angular signature with high biomass conditions. No multi-angle flights were undertaken during SMAPEx-3 as this was not part of the objectives for that campaign.

5) Multi-Azimuth Flights: Since SMAP will make use of a rotating mesh antenna to provide radar observations over the entire swath at a constant incidence angle, it is important to understand what effect the azimuth view angle might have on the radar backscatter values, especially if retrievals will be based on change detection or time series approaches. Consequently, multi-azimuth radar observations were collected during SMAPEx-2 over two focus areas, with the azimuthal incidence angle varying from 0°–180° at 30° increments. Flights were performed at a 1,500 m altitude to maximize the sensitivity of the PLIS radar to potentially weak changes in backscatter with azimuth. The focus areas, approximately 1 km in diameter, included a uniform grassland field and a heterogeneous field comprised of a mix of row crops (corn and wheat), native pasture and bare soil (see locations in Fig. 1). No multi-azimuth flights were undertaken during SMAPEx-1 or SMAPEx-3 as this was not part of the objective for those campaigns.

6) Multi-Resolution Flights: The multi-azimuth flight circuit described above was repeated three times with different settings for the PLIS radar (different pulse bandwidth and digital decimation) so as to image the same ground swath at three different slant range resolutions: 6, 60, and 180 m (azimuth resolution was unchanged at 0.5 m), resulting in ground resolutions at the center of the swath of 12, 120, and 380 m, respectively. These flights provided data to address the scaling of radar observations, which will be crucial to up-scaling of SMAPEx data to a 3 km radar product, and to relate the airborne data to different sources of radar data, such as those of PALSAR [43].

7) PALSAR Transect: An additional radar-only mapping flight was conducted at the beginning of SMAPEx-1 (July 5) to coincide with the overpass of PALSAR, with the objective of providing cross-validation data between PALSAR and PLIS. A focus transect was mapped from a 3000 m altitude, measuring 11–29 m resolution radar backscatter over an 8 km × 22 km area comprising of irrigated crops and grazing land (see Fig. 1). The flight line direction and separation were set so as to

TABLE II
SUMMARY STATISTICS OF THE SMAPEX GROUND MEASUREMENTS FOR THE MAJOR LAND COVER TYPES MONITORED. (*) ONLY ONE MEASUREMENT TAKEN. NOTE: MINIMUM AND MAXIMUM VWC VALUES FOR EACH VEGETATION TYPE WERE EXTRACTED FROM THE RESPECTIVE POPULATION OF INDIVIDUAL DESTRUCTIVE SAMPLES (i.e., NOT AVERAGED BY FIELD)

		Vegetation		Surface roughness				0-5cm soil moisture	
Experiment	Vegetation type	Water content [kg/m^2] min-max	Dry biomass [kg/m^2] min-max	mean RMS height [cm]	Std RMS height [cm]	mean corr. length [cm]	Std corr. length [cm]	mean [m^3/ m^3]	std [m^3/ m^3]
SMAPEx-1	Wheat	0.04-0.04	0.01-0.01	0.4	0.0 (*)	5	0.0 (*)	0.28	0.06
	Maize	*absent*							
	Barley	0.10-0.14	0.03-0.10	0.9	0.1	10.8	4.4	0.23	0.06
	Canola	0.19-0.46	0.08-0.47	0.8	0.2	15.4	10.4	0.24	0.07
	Pasture	0.12-0.81	0.12-1.07	0.7	0.4	25.9	21.1	0.24	0.07
	Bare	-	-	1.7	0.0 (*)	16.2	0.0 (*)	0.23	0.09
SMAPEx-2	Wheat	0.22-0.65	1.12-1.78	1.2	0.3	18	15.2	0.30	0.08
	Maize	1.40-4.0	0.42-1.36	1.1	0.4	13.9	15.7	0.30	0.07
	Barley	0.07-1.13	0.42-1.24	0.8	0.2	17.3	8.5	0.26	0.07
	Canola	*absent*							
	Pasture	0.01-2.19	0.09-0.97	0.8	0.3	31.6	19.2	0.28	0.08
	Bare	*absent*							
SMAPEx-3	Wheat	0.16-2.53	0.07-1.13	1.2	0.5	6.6	6.7	0.14	0.11
	Maize	*absent*							
	Barley	0.16 – 1.8	0.1 – 0.48	1.4	0.4	4.1	2.2	0.12	0.05
	Canola	2.78-7.71	0.33-1.74	1.0	0.2	5.4	1.6	0.29	0.12
	Pasture	0.07-0.95	0.05-1.23	1.0	0.8	11.7	8.2	0.10	0.07
	Bare	-	-	1.9	1.3	9.1	8.0	0.18	0.12

replicate the PALSAR inclination (98°) and provide continuous coverage of radar backscatter between 30°–40° incidence angle, closely matching the PALSAR incidence angle (34°). Although a Transect flight was undertaken during SMAPEx-2, the planned December 7 PALSAR overpass was not acquired by ALOS. During SMAPEx-3 no Transect flights were undertaken as PALSAR was no longer operational.

8) LiDAR and Hyperspectral Flights: LiDAR and hyperspectral observations of selected agricultural and grazing areas were undertaken toward the beginning and end of SMAPEx-3 (September 5 and 22, 2011). The main objective of these flights was to support the ground monitoring of vegetation dynamics, in particular crop plant heights and VWC. Thus, two agricultural focus areas (YA4 and YA7) and one grazing area (YB7) were monitored on both dates from a 400 m altitude (Fig. 1). The LiDAR sensor was operated with 180 kHz pulse repetition frequency, ensuring a density of 8 points per square meter, whereas the hyperspectral sensor was set to a 12 nm spectral and 0.8 m spatial resolution. On the same dates a low altitude (100 m) LiDAR flight was undertaken along a 3 km long, 75 m wide transect in the YA4 focus area characterized by three adjacent bare soil fields with varying surface roughness conditions. At this altitude the LiDAR data had a density of 32 points per square meter. Ground measurements of surface roughness were undertaken at three locations on each field falling within the swath for cross-comparison with the LiDAR roughness estimates.

B. Ground Measurements

Spatial ground sampling was undertaken on every day of airborne monitoring at two of the six 3 km × 3 km focus areas, chosen to represent the diverse land surface conditions in the study area while matching a pixel of the nominal 3 km grid of the SMAP active-only product. The following sections describe the ground data and sampling strategies adopted. Summary statistics of the soil moisture and ancillary data presented by major land cover types are shown in Table II.

1) Spatial Soil Moisture Data: The six focus areas were sampled on rotation with two focus areas sampled for each Regional flight day: one irrigated cropping (YA4, YA7, or YD) and one grazing (YB5, YB7, or YC) area each day. As a result, each focus area was sampled once only during each

TABLE III
CHARACTERISTICS OF GROUND SAMPLING FOCUS AREAS AND SOIL MOISTURE SAMPLING SCHEDULES FOR THE THREE SMAPEX EXPERIMENTS

Area	Land use	SMAPEx-1	SMAPEx-2	SMAPEx-3
		Dates (spacing)	Dates (spacing)	Dates (spacing)
YA4	Irrigated cropping, some grazing	July 6 (250m) July 9 (50m)	Dec 4 (250m) Dec 5, 7 (50m)	Sept 5 (250m) Sept 13 (250m) Sept 19 (250m)
YA7	Irrigated cropping, dryland cropping, some grazing	July 10 (250m)	Dec 8 (250m)	Sept 10 (250m) Sept 18 (250m) Sept 23 (250m)
YD	Irrigated cropping, dryland cropping, some grazing	July 8 (250m)	Dec 6 (250m)	Sept 7 (250m) Sept 15 (250m) Sept 21 (250m)
YC	Grazing	July 8 (250m)	Dec 4 (250m)	Sept 5 (250m) Sept 13 (250m) Sept 19 (250m)
YB5	Grazing	July 7 (50m), July 10 (250m)	Dec 6 (250m)	Sept 10 (250m) Sept18 (250m) Sept 23 (250m)
YB7	Grazing	July 6 (250m)	*Not sampled due to flood*	Sept 7 (250m) Sept 15 (250m) Sept 21 (250m)

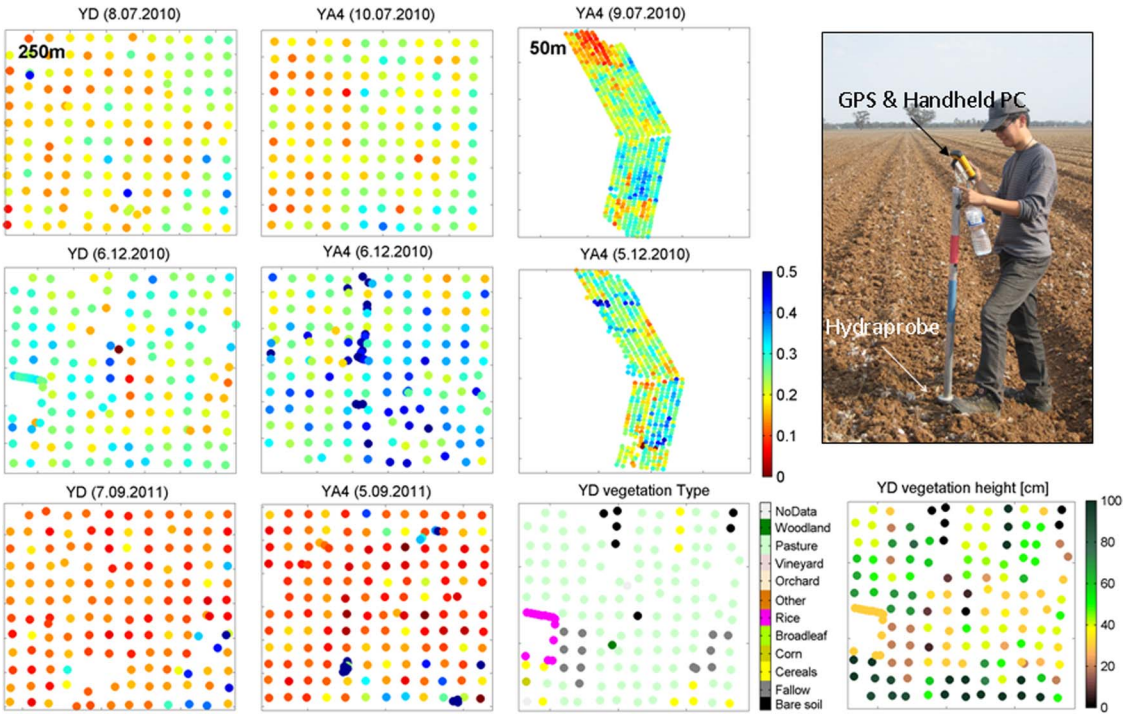

Fig. 5. Sample of the spatial soil moisture data showing: (a) Soil moisture measured at the YD and YA4 areas during SMAPEx-1 (top row), SMAPEx-2 (middle row) and SMAPEx-3 (bottom row), (b) The 50 m resolution transects for YA4 area during SMAPEx-1 (top row) and SMAPEx-2 (middle row), (c) The visual observations of vegetation type and height collected at YD during SMAPEx-2 (bottom row), and (d) The physical setup of the HDAS system is (image to the right). All panels represent areas of 3 km × 3 km in size.

of SMAPEx-1 and -2, and three times during SMAPEx-3. A detailed sampling schedule is shown in Table III, whereas the focus area locations are shown in Fig. 1. For each Target flight, sampling was undertaken along a narrow strip in either YA4 or YB5 accordingly. A sample of the soil moisture data collected is shown in Fig. 5. The 0–5 cm soil moisture measurements were made using the Hydraprobe Data Acquisition System, HDAS [44], which integrates a dielectric probe and a GPS receiver in a mobile GIS environment (see Fig. 5). Spatial measurements were made over an entire 3 km × 3 km focus area on a 250 m spaced grid during Regional flights, and over a 500 m × 3 km portion of the focus area at 50 m spacing along 10 transects each 100 m apart during Target flights (see Fig. 5). Three replicate measurements were taken at each grid node to account for small-scale soil moisture variation. The calibration approach described in Merlin *et al.* [44] was applied to the dielectric measurements and verified using gravimetric samples. During SMAPEx-2, extensive areas of ponded water restricted access to YB5 and YB7, meaning that Target sampling was restricted to YA4, and Regional sampling of YB7 was not undertaken.

Fig. 5 shows the soil moisture maps acquired using the HDAS system together with the information on vegetation type and height collected by the HDAS operators. The soil moisture maps exhibit significant spatial variation due to the different irrigation regimes and vegetation cover variability. The fine resolution (50 m) sampling reveals small scale features associated with field-to-field soil moisture changes.

Spatial soil moisture measurements during SMAPEx were complemented by a network of continuous soil moisture monitoring stations. The permanent soil moisture sites of the Murrumbidgee network (OzNet) measure the soil moisture at 0–5 cm, 0–30 cm, 30–60 cm, and 60–90 cm with a Stevens Water Hydraprobe and Campbell Scientific CS616 water reflectometers, precipitation using a tipping bucket rain gauge, and soil temperature. This network was upgraded in 2010 with 24 semi-permanent near-surface sites measuring 0–5 cm soil moisture with the Stevens Water Hydraprobe and soil temperature at 1, 2.5, and 5 cm. During the experiments, four temporary sites were installed to continuously record soil moisture profiles (0–5 and 20–25 cm), vegetation skin temperature using infrared, and soil temperature (2.5, 5, 15, 40 cm) for accurate estimation of the microwave effective temperature, as well as leaf wetness and rainfall monitoring. The temporary sites were installed on the major vegetation types: wheat, fallow, lucerne and pasture (SMAPEx-1); wheat, corn, native and improved pasture (SMAPEx-2); and canola, wheat, fallow and bare soil (SMAPEx-3). A sample of the continuous monitoring stations data is shown in Fig. 2.

2) Ancillary Data: Ancillary information on land cover, vegetation type, vegetation height, dew presence and irrigation type was collected at each HDAS location by visual inspection. A sample of these is shown in Fig. 5 alongside soil moisture data. Vegetation destructive samples for biomass and water content determination were collected for each major vegetation type in the study area (1–5 samples per each vegetation type) by a dedicated vegetation team. At each destructive sample location, vegetation height, crop row spacing and direction were recorded. Additionally, Leaf Area Index (LAI) and spectral reflectance were also measured at 25 locations distributed on a 10 cm spaced regular grid centered around the location of the destructive sample. Reflectance was measured using a CROPSCAN MSR16R multi-spectral radiometer, set up to measure 8 bands between 470–1640 nm, which matched the MODIS 1–6 bands as well as the 4 visible, infrared and the lower short wave infrared band of the Skye airborne sensors. Surface roughness height and correlation length were measured at 1–3 locations per major vegetation type using two perpendicular 3 m profiles (E-W and N-S directions). During the 1-week long SMAPEx-1 and -2 experiments, vegetation and roughness were sampled under the assumption that no significant changes in vegetation and surface roughness conditions occurred during the sampling period. During SMAPEx-3, vegetation sampling sites were revisited every week to track changes in VWC and biomass. Surface roughness measurements were also repeated at some reference sites at the end of the sampling period to check for wind and/or rainfall induced changes. Moreover, detailed information on soil tilling and plowing was recorded for all focus areas.

During SMAPEx-3, intensive vegetation structure sampling was undertaken at four focus fields representative of the vegetation types present in the study area (canola, pasture and two wheat fields at different growth stages), with the objective of collecting detailed information on plant structure and geometry for discrete radar scatter modeling. Each field was revisited weekly totaling three times during the experiment, thereby capturing the crop structure evolution during the growing season. Plant structure parameters were monitored for each field at 10 uniformly distributed locations. Observations included information on plant density and height, leaf parameters such as water content, dimensions and angle, and stalk water content, length, diameter and angle. These data were supplemented by information on row orientation and spacing, soil moisture, and surface roughness.

Additional sampling of standing water area was performed during SMAPEx-2 to provide data for the development of water body retrieval techniques using SMAP radar observations. The boundaries of nine areas presenting surface water, ranging in size from 10 m^2–0.2 km^2, were mapped using GPS in the YB Target area, with information on vegetation type, height, fraction cover and water depth recorded.

V. Data Overview

A. Radar and Radiometer Calibration

The accuracy of the PLMR radiometer was assessed against hot (blackbody box) and cold (clear sky) calibration targets before and after each SMAPEx flight, as well with in-flight calibration by low altitude passes of a water body where water temperature and salinity were monitored (Lake Wyangan). The radiometer accuracy was estimated to be better than 0.7 K for H-polarization and 2 K for V-polarization including system noise and in flight calibration drift [45].

Calibration of the PLIS radar was performed using a combination of six trihedral Passive Radar Calibrators (PRC's), deployed across-swath in homogeneous grassy fields, and a distributed forest target (forest), imaged each day at both the beginning and end of the scientific monitoring flights to check for calibration drift. PLIS crosstalks and cross-polarized channel imbalances were calculated from the forest data, whereas the PRC data were used to estimate the co-polarized channel imbalances. Absolute radiometric calibration parameters were then estimated as the difference between the measured PRC backscattered power and the theoretical radar cross-section for the trihedral-shaped PRC. After polarimetric and radiometric calibration, the measured PRC backscattered exhibited a mean HH-VV amplitude ratio of 1 and mean phase differences of $2.8^\circ(\pm 4.9^\circ)$ and $6.3^\circ(\pm 4.9^\circ)$ for the left and right antenna, respectively. The absolute radiometric calibration coefficients estimated independently for the PLIS right and left antennas were -30.6 dB and -31.5 dB (SMAPEx-1), -30.2 dB and -30.2 dB (SMAPEx-2) and -30.9 dB and -32.3 dB (SMAPEx-3), highlighting a good long-term stability of the PLIS instrument. The coefficients varied with a standard deviation of 0.8 dB over the 3-weeks long SMAPEx-3 experiment. After radiometric calibration, the difference between observed

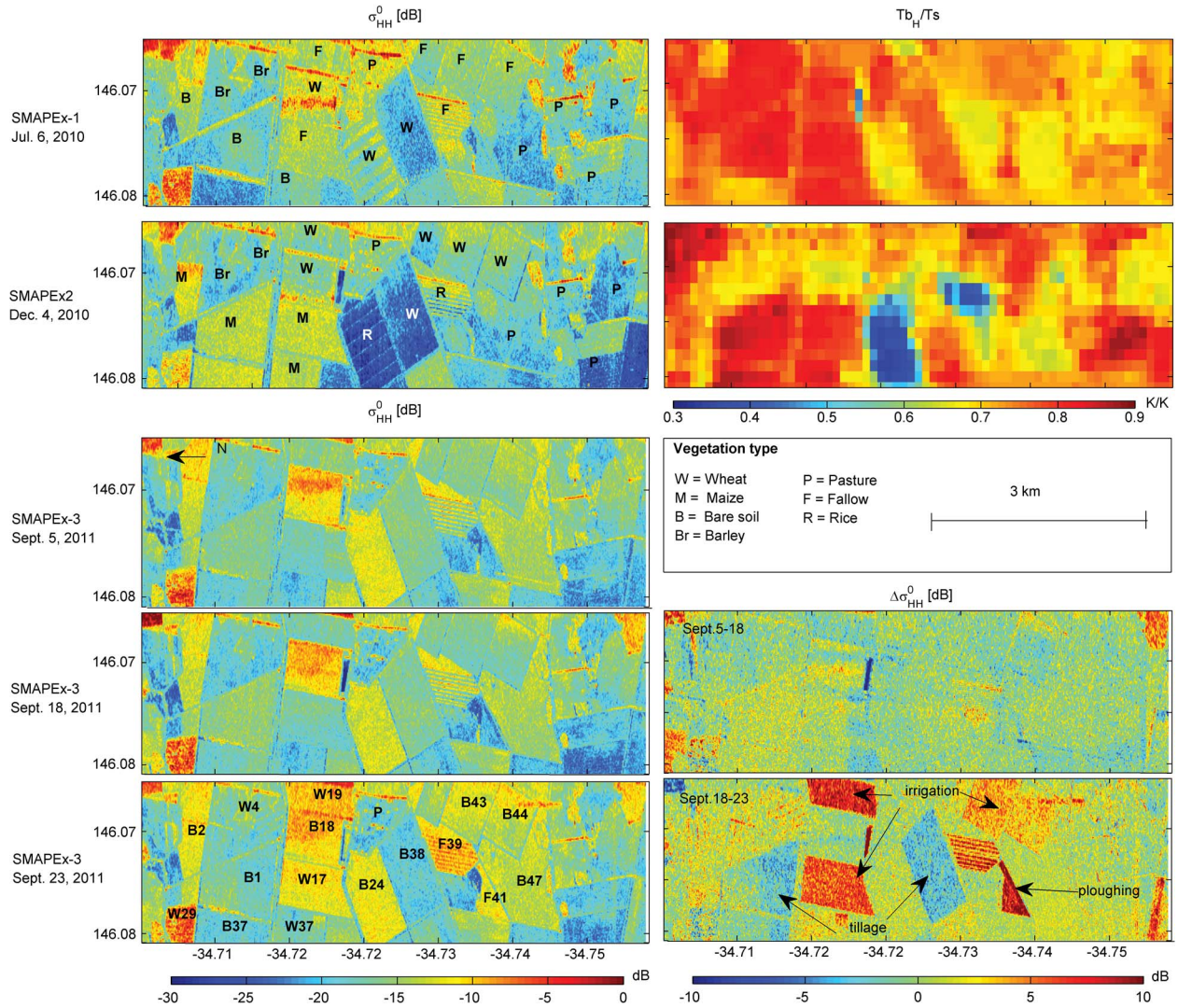

Fig. 6. Example of airborne L-band radar backscatter in HH polarization (σ^0_{HH}, left panels) and radiometer brightness temperatures in H polarization ($\mathrm{Tb_H}$, top—right panels) collected during the SMAPEx-1 and SMAPEx 2 experiments (Target flights) and on 3 dates during SMAPEx-3 (Regional flights). The bottom 2 panels on the right show the date-to-date backscatter change ($\Delta\sigma^0_{\mathrm{HH}}$). for the SMAPEx-3 dates. The radar single-look data were multi-looked by a factor of 2 (range) $\times$ 14 (azimuth) and then resampled to a 10 m grid. Radiometer data were gridded to a 100 m regular grid and normalized by the area average soil temperature (extracted from the ground monitoring stations).

and theoretical PRC cross section was on average 0.93 dB (absolute radiometric accuracy) with a standard deviation of 0.8 dB (relative radiometric accuracy). As a comparison, PALSAR relative radiometric accuracy is 0.76 dB [46].

B. Sensitivity of Microwave Observations to Surface Conditions

This section presents an assessment of the sensitivity of the active and passive microwave observations collected during the SMAPEx experiments to land surface conditions. Fig. 6 presents maps of the radar backscatter coefficient for HH-polarization (σ^0_{HH}) collected during the three SMAPEx experiments over a portion of the YA target area characterized by intensive irrigation cropping. High resolution (100 m) radiometer brightness temperatures at H-polarization ($\mathrm{Tb_H}$) are also shown for SMAPEx-1 and -2, where high resolution Tb data were available from Target flights. It should be noticed that the area displayed is approximately 6 $\times$ 3 km in size, being only a small portion of the total area monitored. Neverthelss, it is representative of the surface conditions experienced during the SMAPEx experiments. The backscatter data shown are polarimetrically and radiometrically calibrated, and are expressed in decibels (dB). The radar single-look data were multi-looked by a factor of 2 (in range) and 14 (in azimuth) to achieve a similar azimuth and range resolution of approximately 12 m, and then resampled to a 10 m grid. Brightness temperature data were gridded to a 100 m regular grid and normalized by the average soil temperature for the area (average between the ground monitoring stations), so as to represent a proxy of the surface emissivity, independent from seasonal changes in soil temperature between experiments.

Significant spatial patterns and temporal changes in σ^0 and emissivity ($\mathrm{Tb_H/Ts}$) can be observed in association with changes in surface conditions such as vegetation cover and soil moisture. Fairly homogeneous σ^0 and emissivity were observed

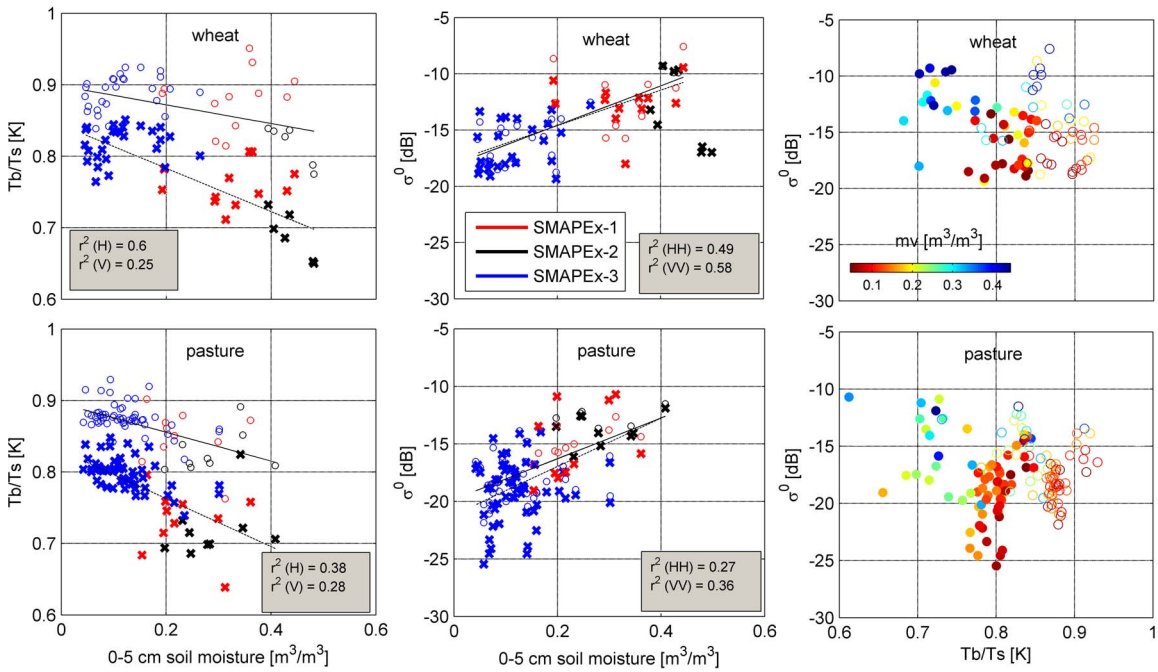

Fig. 7. Radiometer brightness temperatures (Tb) and radar backscatter coefficient (σ^0) plotted against the volumetric soil moisture (mv) in the top 0–5 cm (left and middle panels, respectively) and compared with each other (right panels). Data from all SMAPEx experiments are included in the plot with vertically (circles) and horizontally (crosses) polarized channels shown. Regression lines and respective correlation coefficients (r^2) are calculated on the merged data set for V (dashed lines) and H (continuous lines) channels. Radar and radiometer data are aggregated to the same ground resolution (1 km for SMAPEx-3, 100 m for SMAPEx-1 and 2). The dominat vegetation type was used to classify each pixel. All available ground soil moisture measurement (16 on average) are averaged for each 1 km pixel. Tb were normalized using the ground measured soil temperature (Ts) to remove differences in observed Tb due to seasonal Ts changes.

during SMAPEx-1, at the inset of the crop growing season and with generally low biomass conditions. During SMAPEx-2, moist conditions and elevated biomass of maize and wheat determined a stronger spatial variability in σ^0 and emissivity. Maize exhibited both high σ^0 and emissivity associated with the elevated VWC (see Table II), whereas wheat and barley, being in a senescent stage, were both characterized by lower σ^0 and emissivity. Fig. 6 shows the different interplay between soil moisture and VWC in determining σ^0 and emissivity. Although both maize and barley fields in the northern part of the area (left of the image) were wetter during SMAPEx-2 than during SMAPEx-1, this resulted in a decrease of emissivity only for the barley fields (lower VWC). Conversely, the increase in vegetation biomass on the bare fields in SMAPEx-1, which were characterized by mature maize fields in SMAPEx-2, compensated for the increase in soil moisture with no appreciable change in emissivity could detected. Radar backscatter was fairly constant between July and December on the barley fields but increased significantly for the maize fields, indicating a significant sensitivity of σ^0 to VWC changes. The wetter conditions experienced during SMAPEx-2 are also reflected in an overall decrease in $\mathrm{Tb_H}/\mathrm{Ts}$ between SMAPEx-1 and -2, particularly over pasture and fallow areas. Also, notable is the presence of flooded rice fields during SMAPEx-2, determining a strong decrease in both σ^0 and emissivity. During SMAPEx-3 the area was mostly bare or cultivated at wheat, with significant spatial and temporal variability of σ^0 associated to irrigation and farming practices (see date-to-date $\Delta\sigma^0$ bottom right panels in Fig. 6.

The synergy between active and passive microwave observations during the SMAPEx experiment and their relationship with soil moisture is shown in Fig. 7, where the radiometer brightness temperatures (normalized by the soil temperature Ts) and radar backscatter are plotted against the ground-measured soil moisture (0–5 cm). Radar data were aggregated to the radiometer resolution to allow direct comparison between the two sensors. For SMAPEx-1 and -2, the Target flights were used due to the high radiometer resolution (100 m). Given the absence of high resolution target flights during SMAPEx-3, Regional flights data at 1 km resolution are showed for SMAPEx-3. To allow a meaningful comparison between the data collected during the three SMAPEx experiments, data are presented for the 2 vegetation types which covered the largest fraction of the study area and were present in all 3 experiments (wheat and pasture). It is worh mentioning that, since each SMAPEx-3 data point in Fig. 7 represents the integrated response of a 1×1 km area, some data points might contain a variety of surface types beside the dominant one indicated here. This is particularly the case for the wheat fields in the irrigated area (YA, see Fig. 6). A significant relationship can be observed between Tb and soil moisture for both land cover types and across the SMAPEx experiments, with a decrease in Tb associated to increasing soil moisture due to the decrease in emissivity of wet soils. The slope of the relationship is higher for H than for V polarization, indicating higher sensitivity to soil moisture for $\mathrm{Tb_H}$, as observed in several previous studies. The scattered data points observed mainly in the SMAPEx-2 data were associated to very localized features like water dams and group of trees, picked up by the high resolution radiometer data. The backscatter coefficient σ^0 exhibits sensitivity to soil moisture, although a large scatter is notable in the data. This is likely an effect of the spatial heterogeneity of factors affecting

the backscatter such as VWC and surface roughness. The relationship between Tb, σ^0 and soil moisture shows consistency between the experiments, and it is notable how the data from the 3 experiments complement each other to allow the observations of a wider range of soil moisture conditions than taken individually. In the right panels of Fig. 7 it is shown that the relationship between Tb and σ^0 overall follows the expected variation due to soil moisture changes, which can be exploited for testing of algorithms for retrieval of soil moisture from active and passive microwave observations.

One of the main objectives of the 3-week long SMAPEx-3 experiment was the collection of dense time series of radar data to allow testing of change detection techniques for the SMAP mission. An overview of the temporal dynamics of σ^0 observed during the 3-week long SMAPEx-3 experiment is given in the right panels in Fig. 6, where difference in $\sigma^0_{\rm HH}$ between each date are displayed. It should be noted that a large percentage of the fields monitored during SMAPEx-3 ($\sim$70%) exhibited a narrow soil moisture dynamic range (< 0.1 m^3/m^3), with significant soil moisture dynamics limited to irrigated fields. This is visible in Fig. 2 and is reflected in the very small change of backscatter observed across the area in Fig. 6 between September 5 and 18. Between September 18 and 23, farming activities took place at various fields resulting in noticeable changes in σ^0. Flood Irrigation of the wheat fields W#17 and W#19 for example determined an increase in $\sigma^0_{\rm HH}$ of $\sim$7 dB whereas surface roughness changes due to tillage at the bare fields B#1 and B#38 resulted in a decrease of $\sim$3 dB for $\sigma^0_{\rm HH}$. Different tillage practices also determine differences in $\sigma^0_{\rm HH}$ within the same land cover type: For very similar soil moisture conditions (~ 0.1 m^3/m^3), a 2 dB backscatter difference was observed for bare soil fields (#47 and #38) characterized by different surface geometric properties: isotropic roughness due to soil clods and periodic row structure, respectively.

Fig. 8 displays examples of time series of $\sigma^0_{\rm HH}$, $\sigma^0_{\rm VV}$ and $\sigma^0_{\rm HV}$ and ground soil moisture data (volumetric percent in the 0–5 cm layer) recorded during the SMAPEx-3 experiment to assess the response of the different radar channels to changes in surface and vegetation conditons. Six fields were chosen among all those monitored to present the range of conditions encountered in the SMAPEx study area. It is observed that the backscatter coefficient exhibits a positive correlation to soil moisture conditions for all vegetation types, with σ^0 increasing in response to increasing soil moisture. A reasonable response of σ^0 to soil moisture change is also observed at fields with high biomass like the wheat and canola fields, the latter exhibiting the highest VWC encountered during the SMAPEx experiments (up to 7 kg/m^2, see Table II). The most notable impact of the increasing VWC is the change in co-polarized ratio $\sigma^0_{\rm HH}/\sigma^0_{\rm VV}$. This comes mainly as a result of a decrease in $\sigma^0_{\rm VV}$, which could be explained by the attenuation of the signal due to the predominance of vertically oriented scatterers in crop plants. However, differences in incidence angles between the bare and vegetated fields might also play a role in decreasing $\sigma^0_{\rm VV}$. Notice that as a consequence of the decrease in $\sigma^0_{\rm VV}$, at elevated VWC (i.e., the wheat and canola fields), $\sigma^0_{\rm HH}$ becomes higher than $\sigma^0_{\rm VV}$. This is not expected from theoretical models of bare surface scattering, which predict $\sigma^0_{\rm HH}$ always lower than

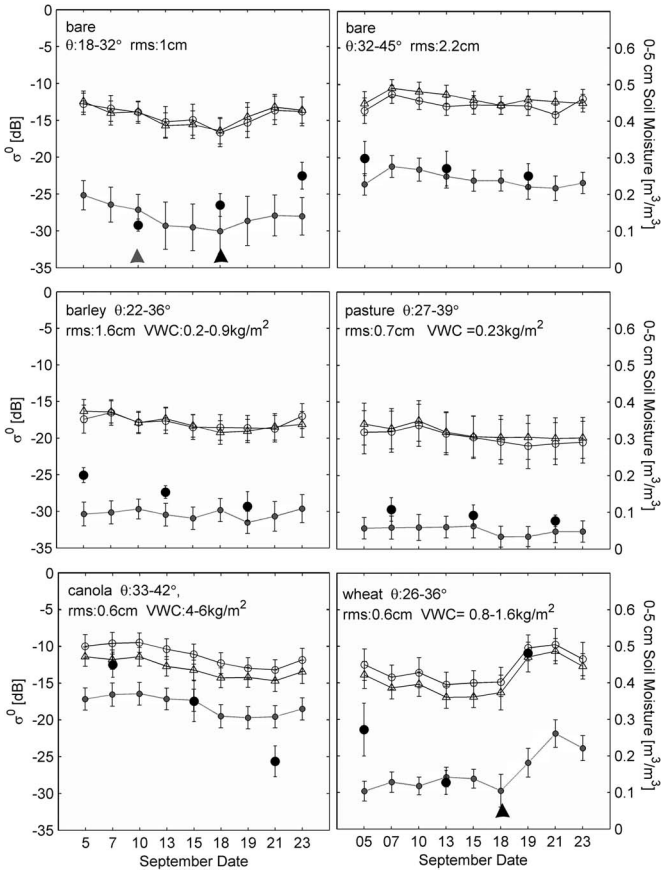

Fig. 8. Time series of L-band backscatter coefficients σ^0 (dotted lines) and soil moisture measurements (dots) plotted daily at six field fields with vegetation type, incidence angle (θ), surface roughness Root Mean Square (rms) and Vegetation Water Content (VWC) as indicated in each panel. Backscatter coefficients are shown for HH-pol (hollow circles), VV-pol (hollow triangles) and HV-pol (gray filled circles). Each data point represents the average and standard deviation of the backscatter coefficient and soil moisture values within the field. Dates when farming activities were recorded on each field are also shown at the bottom of the respective panel for irrigation (black filled triangles) and tillage (gray filled triangles).

$\sigma^0_{\rm VV}$ at off-nadir angles, but could depend on the interaction between vegetation elements and the soil surface and has been observed in other experiments over corn fields of similar VWC [14]. A second notable impact of increasing VWC values is the decrease of the difference between $\sigma^0_{\rm HV}$ and $\sigma^0_{\rm VV}$ as a consequence of both a decrease in $\sigma^0_{\rm VV}$ and an increase in $\sigma^0_{\rm HV}$. For the canola field, which was already well developed at the beginning of the experiment, the $\sigma^0_{\rm HV} - \sigma^0_{\rm VV}$ [dB] difference was small and fairly constant throughout the experiment. However, for the wheat field the $\sigma^0_{\rm HV} - \sigma^0_{\rm VV}$ [dB] difference is seen to decrease gradually during the experiment. Since the VWC of the wheat fields increased throughout the experiment, this might be the result of an increase in canopy volume scattering in HV polarization. An example of the response of σ^0 to changes in surface roughness associated with farming activities is shown in the top-left panel of Fig. 8. $\sigma^0_{\rm HV}$ appears to be more sensitive to changes in surface roughness due to tillage than the co-polarized σ^0. This indicates the potential for using the co-cross-polarization ratio (e.g., $\sigma^0_{\rm HV}/\sigma^0_{\rm VV}$) to map such changes in the context of change detection techniques.

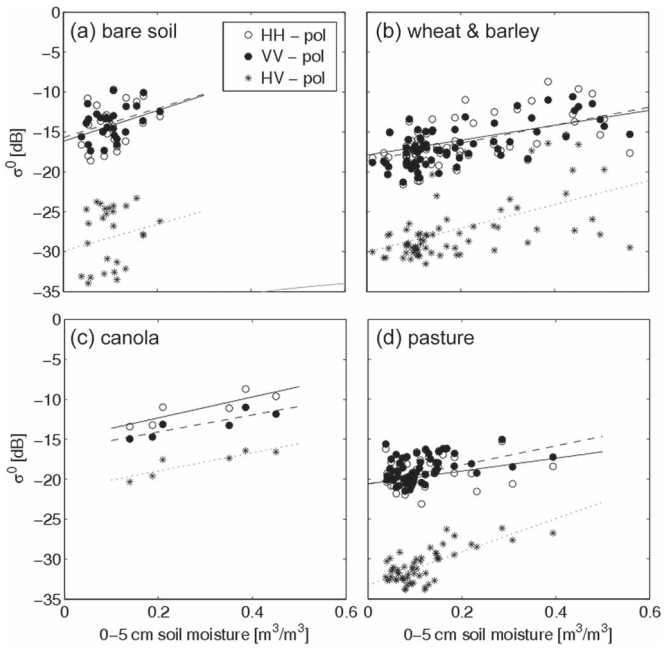

Fig. 9. Scatter plot between backscatter coefficient (σ^0) and volumetric soil moisture in the top 0–5 cm for all the fields monitored during SMAPEx-3 in focus areas YA4, YA7, YC and YD. For each field, the daily averages σ^0 and soil moisture calculated across the field area for each of the 3 sampling dates are plotted. Bare soils where changes in surface conditions were recorded due to tillage or ploughing were excluded from the plot. Linear regression lines are shown for polarizations HH (continuous line), VV (dashed line) and HV (dotted line). Regression statistics are reported in Table IV.

Fig. 9 presents scatter plots of the daily field-average σ^0 and soil moisture for all the fields monitored during SMAPEx-3. Field-average values were used to reduce noise in the relationship due to soil moisture sampling error and small-scale spatial variability. The scatter plots indicate a positive correlation between σ^0 and soil moisture for all vegetation types, with the slope of the relationship being highest for bare fields and generally lower for vegetated soil. The regression statistics for the scatter plots in Fig. 9 are reported in Table IV. The sensitivity of σ^0 to soil moisture (expressed in units of decibel per unit volumetric soil moisture, "dB/m^3/m^3") ranged between 0.19 dB/m^3/m^3 for bare fields to 0.05 dB/m^3/m^3 for pasture in HH polarization, with cereals and canola fields exhibiting intermediate sensitivities of 0.11 and 0.13 dB/m^3/m^3, respectively (HH-pol). Such sensitivities correspond roughly to a difference in σ^0 between very dry and near-saturation conditions (0.4 m^3/m^3) of 7.6, 4.2, 5.2, and 2 dB for bare, cereals, canola and pasture fields, respectively. No significant differences in sensitivity could be observed between the radar channels. The observed sensitivity of σ^0 for pasture fields is unexpected and inconsistent to what observed in Fig. 7. However, this is not entirely suprising when considering that the majority of pasture fields exhibited very small soil moisture dynamic range during SMAPEx-3 (0.08 m^3/m^3 on average over 3-weeks), whereas in Fig. 7 the SMAPEx-1 and -2 data points provide with a wider range of soil moisture conditions. Moreover, when the analysis is restricted to small dynamic ranges the impact of the radar short-term calibration stability and the within field spatial variability might disrupt the correlation between σ^0 and soil moisture, as can be appreciated in the example of radar timeseries for a pasture field shown in Fig. 8.

The fairly low correlation coefficients reported in Table IV for bare soils and wheat is associated to the significant dispersion visible in Fig. 9. When many fields are plotted together, noise in the relationship between σ^0 and soil moisture can arise due to variations in vegetation water content and surface roughness between fields. To overcome this problem, the backscatter sensitivity to soil moisture is recalculated in Table IV after grouping the data points according to VWC and surface roughness. To this end, data from the vegetation and surface roughness ground sampling were used to classify each field, after which the regression analysis was repeated with the data points pooled into each VWC or roughness subset. Note that this significantly decreases the number of fields available for the analysis given that not all the fields measured for soil moisture were sampled for vegetation and surface roughness. Therefore, the adjusted coefficient of determination (R^2) is shown to account for the statistical significance of the sample population. The correlation coefficients improved when considering subsets of data points based on VWC, indicating that the scatter in Fig. 8 for wheat and barley is partially due to VWC variation between fields. When restricting the attention to the VWC classes where a good correlation is observed, the sensitivity of σ^0 soil moisture tends to decrease from 0.17 to 0.24 dB/m^3/m^3 for VWC ranging 0.5–1 and 1–1.5 kg/m^2 (wheat fields) to 0.13 dB/m^3/m^3 for VWC $\sim$ 5 kg/m^2 (average VWC of canola fields). For the lower VWC ranges ($<$ 1 kg/m^2), the correlation remained poor. However, these were non-irrigated pasture and wheat fields with narrow soil moisture dynamic ranges. Another issue potentially affecting these results is the representativeness of the ground soil moisture measurements (taken on 250 m grid) as an estimate of the average soil moisture of fields sized from 1–50 ha.

Grouping the fields by surface roughness slightly improved the correlation between σ^0 and soil moisture for low roughness classes (0.5–1.3 cm rms). There appears to be a decreasing trend in sensitivity of σ^0 with increasing surface roughness and a loss of correlation when surface roughness reaches 1.3–2 cm rms. However, it should be noticed that the two classes with highest roughness included data points with small dynamic range. Moreover, the agricultural fields in SMAPEx-3 included a variety of row structure and isotropic surfaces, which was seen in Fig. 6 to have an impact on the backscatter. Further analysis will be required to understand the impact of different crop row direction on the backscattered signal which is, however, beyond the scope of the data overview presented here.

VI. Summary

The SMAP satellite will use combined passive (radiometer) and active (radar) microwave L-band instruments to provide high-resolution radar-only ($\sim$3 km), low-resolution radiometer-only ($\sim$36 km) and intermediate-resolution combined radar–radiometer ($\sim$9 km) soil moisture products globally. The Soil Moisture Active Passive Experiments (SMAPEx) were designed to provide an extensive data set of L-band radar and radiometer airborne observations to serve as an algorithm

TABLE IV
SENSITIVITY OF RADAR BACKSCATTER(σ^0) TO 0–5 cm SURFACE SOIL MOISTURE (mv) FOR THE MAJOR LAND COVER TYPES IN THE SMAPEx AREA. $\Delta\sigma^0_{PP}$ INDICATES THE OBSERVED CHANGES IN σ^0_{PP} (P = polarization) FOR UNIT OF VOLUMETRIC SOIL MOISTURE, CALCULATED FOR INDIVIDUAL FIELDS AS THE SLOPE OF THE LINEAR REGRESSION BETWEEN THE DAILY AVERAGES σ^0 AND SOIL MOISTURE CALCULATED. THE VARIATION IN BACKSCATTER SENSITIVITY WITH INCREASING VEGETATION WATER CONTENT (VWC) AND SURFACE ROUGHNESS ROOT MEAN SQUARE HEIGHTS (rms)

	Sensitivity (=$\Delta\sigma^0_{PP}$/ Δmv*0.01) and [adjusted R^2]				
	Nr. Data points	HH	VV	HV	Notes
Bare soil*	30	0.19 [0.06+]	0.18 [0.10++]	0.17 [0.00]	
Wheat & barley	72	0.11 [0.27++]	0.13 [0.43++]	0.16 [0.29++]	
Canola	6	0.13 [0.69++]	0.11 [0.69++]	0.11 [0.73++]	
Pasture	93	0.05 [0.03]	0.09 [0.14++]	0.20 [0.48+]	
VWC** classes					
VWC [kg/m2]<0.5	9	0.62 [0.18]	0.54 [0.13]	0.44 [0.03]	small dynamic range
VWC [kg/m2]= 0.5 - 1	12	0.08 [0.02]	0.16 [0.25+]	0.03 [-0.08]	small dynamic range
VWC [kg/m2]=1-1.5	6	0.17 [0.89++]	0.16 [0.81++]	0.07 [0.37+]	
VWC [kg/m2]=1.5-2	9	0.24 [0.68++]	0.19 [0.47++]	0.17 [0.62++]	
VWC [kg/m2] > 2	6	0.13 [0.69++]	0.11 [0.69++]	0.11 [0.73++]	
Roughness classes					
0.5 < rms < 0.9 cm	12	0.12 [0.68++]	0.07 [0.48++]	0.12 [0.31++]	
1.3 < rms < 1.6 cm	9	0.20 [0.86++]	0.16 [0.77++]	0.34 [0.69++]	
0.9 < rms < 1.3 cm	9	-0.07 [-0.09]	0.07 [-0.11]	-0.14 [0.09]	small dynamic range
rms > 1.3 cm	9	0.00 [-0.20]	0.10 [0.35]	0.08 [0.29]	small dynamic range

+ Statistical significant with 90% confidence
++ Statistical significant with 95% confidence
* Fields with tillage or ploughing excluded
** Calculated for each field as the average Vegetation Water Content along the experiment period

development test-bed for the SMAP mission. Airborne observations and supporting ground data were collected over an area the size of a SMAP footprint with 2–3 days revisit time to simulate observations expected from SMAP. Additional flights targeted the impact of the spatial scale, as well as incidence and azimuth angle effects on the radar backscatter. Concurrent ground data collection included soil moisture (50 m to 250 m spacing), vegetation biomass and geometric properties, and surface roughness over six 3 km × 3 km areas. The SMAPEx experiments were timed to cover various climatic conditions as well as various stages of the crop growing season, including winter onset (SMAPEx-1), spring growth (SMAPEx-3) and summer senescence (SMAPEx-2). This resulted in the monitoring of a wide range of land surface conditions including full range of soil moisture conditions and vegetation biomass ranging from 0–4 kg/m2. Preliminary analysis of the data was presented, including an assessment of the accuracy of the radiometer and radar calibrations, and the sensitivity of the collected active and passive microwave data to changes in soil moisture and vegetation conditions. A good sensitivity of passive microwave data to soil moisture and correlation between active and passive microwave observations was shown for the SMAPEx experiments. The analysis of dense radar temporal series collected during the 3-week long SMAPEx-3 experiment showed that airborne radar data were sensitive to changing soil moisture conditions, vegetation water content and changes in surface roughness due to farming practices. Other features highlighted in the data which will deserve more in-depth analysis than possible in the contest of this study include the effect of vegetation on the backscatter polarization ratios, the impact of tillage on the radar backscater temporal series and the effect of spatial heterogeneity on the relationship between radar backscatters and soil moisture. This preliminary analysis has confirmed the potential of the SMAPEx data set to address a variety of SMAP prelaunch science question. SMAPEx data are publicly available at www.smapex.monash.edu.au.

ACKNOWLEDGMENT

The authors wish to thank N. Stacey and A. Goh at the Defence Science and Technology Organisation (DSTO), for assisting with the PLIS radar initial testing and deployment

and for providing a calibration package, B. Bates at DSTO for arranging the radar spectrum license, G. Beecher at the Yanco Agricultural Institute (YAI), Yanco NSW, for providing access to their facilities and general support during the experiments, and A. McGrath and W. Lieff at Airborne Research Australia for undertaking the LiDAR and hyperspetral flights. The authors also wish to thanks Y. Nan at Monash University for undertaking the normalization of the PLIS data. Thanks also to all the SMAPEx experiment participants: M. Ahmad, A. Balenzano, R. Bindlish, M. Bürgin, S. Chai, C. Cheong, S. Chua, A. Colliander, I. Davenport, K. Fieber, P. Hamel, S. Hasan, L. Huang, D. Jinyang, J. Johanson, A. Joseph, S. Kim, M. Kurum, K. K. Loh, L. McKee, F. Méndez, P. O'Neill, W. Ooi, J. Ouellette, M. Piles, R. Pipunic, J. Prueger, G. Satalino, C. Vittucci, F. Winston, W. Wong, J. Yeates, M. Yellishetty, and R. Young.

REFERENCES

[1] D. Entekhabi, E. G. Njoku, P. E. O'Neill, K. H. Kellogg, W. T. Crow, W. N. Edelstein, J. K. Entin, S. D. Goodman, T. J. Jackson, J. Johnson, J. Kimball, J. R. Piepmeier, R. D. Koster, N. Martin, K. C. McDonald, M. Moghaddam, S. Moran, R. Reichle, J. C. Shi, M. W. Spencer, S. W. Thurman, L. Tsang, and J. van Zyl, "The soil moisture active passive (SMAP) mission," *Proc. IEEE*, vol. 98, no. 5, pp. 704–716, May 2010.

[2] R. D. Koster, M. J. Suarez, R. W. Higgins, and H. M. Van den Dool, "Observational evidence that soil moisture variations affect precipitation," *Geophys. Res. Lett.*, vol. 30, no. 5, p. 1241, Mar. 2003.

[3] A. Betts, J. Ball, A. Beljaars, M. J. Miller, and P. A. Viterbo, "The land surface-atmosphere interaction: A review based on observational and global modeling perspectives," *J. Geophys. Res. Atmos.*, vol. 101, no. D3, pp. 7209–7225, Jan. 1996.

[4] D. Entekhabi, I. Rodriguez-Iturbe, and F. Castelli, "Mutual interaction of soil moisture state and atmospheric processes," *J. Hydrol.*, vol. 184, no. 1/2, pp. 3–17, Oct. 1996.

[5] W. Wagner, G. Lemoine, and H. Rott, "A method for estimating soil moisture from ERS scatterometer and soil data," *Remote Sens. Environ.*, vol. 70, no. 2, pp. 191–207, Nov. 1999.

[6] E. G. Njoku and L. Li, "Retrieval of land surface parameters using passive microwave measurements at 6–18 GHz," *IEEE Trans. Geosci. Remote Sens.*, vol. 37, no. 1, pp. 79–93, Jan. 1999.

[7] Y. H. Kerr, P. Waldteufel, J. P. Wigneron, J. Martinuzzi, J. Font, and M. Berger, "Soil moisture retrieval from space: The soil moisture and ocean salinity (SMOS) mission," *IEEE Trans. Geosci. Remote Sens.*, vol. 39, no. 8, pp. 1729–1735, Aug. 2001.

[8] W. A. Gallus and M. Segal, "Sensitivity of forecast rainfall in Texas convective systems to soil moisture and convective parameterizations," *Weather Forecast.*, vol. 15, no. 5, pp. 509–525, Oct. 2000.

[9] C. L. Ziegler, W. J. Martin, R. A. Pielke, A. Roger, and R. L. Walko, "A modeling study of the dryline," *J. Atmosp. Sci.*, vol. 52, no. 2, pp. 263–285, 1994.

[10] W. Wagner, G. Bloschl, P. Pampaloni, J.-C. Calvet, B. Bizzarri, J.-P. Wigneron, and Y. Kerr, "Operational readiness of microwave remote sensing of soil moisture for hydrologic applications," *Nordic Hydrol.*, vol. 38, no. 1, pp. 1–20, Jul. 2006.

[11] J. R. Wang and B. J. Choudhury, "Remote sensing of soil moisture content over bare field at 1.4 GHz frequency," *J. Geophys. Res.*, vol. 86, no. C6, pp. 5277–5282, 1981.

[12] T. J. Jackson, T. J. Schmugge, and J. R. Wang, "Passive microwave sensing of soil-moisture under vegetation canopies," *Water. Resour. Res.*, vol. 18, no. 4, pp. 1137–1142, Jan. 1982.

[13] T. J. Jackson, D. M. Le Vine, A. Y. Hsu, A. Oldak, P. J. Starks, C. T. Swift, J. D. Isham, and M. Haken, "Soil moisture mapping at regional scales using microwave radiometry: The southern great plains hydrology experiment," *IEEE Trans. Geosci. Remote Sens.*, vol. 37, no. 5, pp. 2136–2151, Sep. 1999.

[14] E. G. Njoku, W. J. Wilson, S. H. Yueh, S. J. Dinardo, F. K. Li, T. J. Jackson, V. Lakshmi, and J. Bolten, "Observations of soil moisture using a passive and active low-frequency microwave airborne sensor during SGP99," *IEEE Trans. Geosci. Remote Sens.*, vol. 40, no. 12, pp. 2659–2673, Dec. 2002.

[15] P. E. O'Neill, N. Chauhan, and T. J. Jackson, "Use of active and passive microwave remote sensing for soil moisture estimation through corn," *Int. J. Remote Sens.*, vol. 17, no. 10, pp. 1851–1865, Jul. 1996.

[16] T. J. Jackson, R. Bindlish, A. J. Gasiewski, B. Stankov, M. Klein, E. G. Njoku, D. Bosch, T. L. Coleman, C. A. Laymon, and P. Starks, "Polarimetric scanning radiometer C- and X-band microwave observations during SMEX03," *IEEE Trans. Geosci. Remote Sens.*, vol. 43, no. 11, pp. 2418–2430, Nov. 2005.

[17] R. Panciera, J. P. Walker, J. D. Kalma, E. J. Kim, J. M. Hacker, O. Merlin, M. Berger, and N. Skou, "The NAFE'05/CoSMOS data set: Toward SMOS soil moisture retrieval, downscaling and assimilation," *IEEE Trans. Geosci. Rem. Sens.*, vol. 46, no. 3, pp. 736–745, Mar. 2008.

[18] O. Merlin, J. P. Walker, J. D. Kalma, E. J. Kim, J. Hacker, R. Panciera, R. Young, G. Summerell, J. Hornbuckle, M. Hafeez, and T. Jackson, "The NAFE'06 data set: Toward soil moisture retrieval at intermediate resolution," *Adv. Water. Resour.*, vol. 31, no. 11, pp. 1444–1455, Nov. 2008.

[19] F. T. Ulaby, R. K. Moore, and A. K. Fung, *Microwave Remote Sensing: Active and Passive. From Theory to Application*, vol. 3. Norwood, MA, USA: Artech House, 1986.

[20] E. P. W. Attema, "Vegetation modeleld as a water cloud," *Radio Sci.*, vol. 13, no. 2, pp. 357–364, Mar./Apr. 1978.

[21] R. H. Lang and J. S. Sighu, "Electromagnetic backscattering from a layer of vegetation: A discrete approach," *IEEE Trans. Geosci. Remote Sens.*, vol. GRS-21, no. 1, pp. 62–71, Jan. 1983.

[22] A. K. Fung, Z. Li, and K. S. Chen, "Backscattering from a randomly rough dielectric surface," *IEEE Trans. Geosci. Remote Sens.*, vol. 30, no. 2, pp. 356–369, Mar. 1992.

[23] T.-D. Wu and K.-S. Chen, "A reappraisal of the validity of the IEM model for backscattering from rough surfaces," *IEEE Trans. Geosci. Remote Sens.*, vol. 42, no. 4, pp. 743–753, Apr. 2004.

[24] P. C. Dubois, J. V. Zyl, and T. Engman, "Measuring soil moisture with imaging radars," *IEEE Trans. Geosci. Remote Sens.*, vol. 33, no. 4, pp. 915–956, Jul. 1995.

[25] R. Bindlish and A. P. Barros, "Parameterization of vegetation backscatter in radar-based, soil moisture estimation," *Remote Sens. Environ.*, vol. 76, no. 1, pp. 130–137, Apr. 2001.

[26] R. D. de Roo, Y. Du, F. T. Ulaby, and M. C. Dobson, "A semi-empirical backscattering model at L-Band and C-Band for a soybean canopy with soil moisture inversion," *IEEE Trans. Geosci. Remote Sens.*, vol. 39, no. 4, pp. 864–872, Apr. 2001.

[27] Y. Oh, "Quantitative retrieval of soil moisture content and surface roughness from multipolarized radar observations of bare soil surfaces," *IEEE Trans. Geosci. Remote Sens.*, vol. 42, no. 3, pp. 596–601, Mar. 2004.

[28] I. Gherboudj, R. Magagi, A. A. Berg, and B. Toth, "Soil moisture retrieval over agricultural fields from multi-polarized and multi-angular RADARSAT-2 SAR data," *Remote Sens. Environ.*, vol. 115, no. 1, pp. 33–43, Jan. 2011.

[29] U. Narayan and V. Lakshmi, "Characterizing subpixel variability of low resolution radiometer derived soil moisture using high resolution radar data," *Water Resour. Res.*, vol. 44, no. 6, Jun. 2008.

[30] R. Bindlish, T. Jackson, R. Sun, M. Cosh, S. Yueh, and S. DiNardo, "Combined passive and active microwave observations of soil moisture during CLASIC," *IEEE Geosci. Remote Sens. Lett.*, vol. 6, no. 4, pp. 644–648, Oct. 2009.

[31] M. Piles, A. Camps, M. Vall-llossera, and M. Talone, "Spatial resolution enhancement of SMOS data: A deconvolution-based approach," *IEEE Trans. Geosci. Remote Sens.*, vol. 47, no. 7, pp. 2182–2192, Jul. 2009.

[32] X. Zhan, P. R. Houser, J. P. Walker, and W. T. Crow, "A method for retrieving high-resolution surface soil moisture from hydros L-band radiometer and Radar observations," *IEEE Trans. Geosci. Remote Sens.*, vol. 44, no. 6, pp. 1534–1544, Jun. 2006.

[33] U. Narayan and V. Lakshmi, "A simple method for spatial disaggregation of radiometer derived soil moisture using higher resolution radar observations," *J. Electromagn. Waves Appl.*, vol. 19, no. 13, pp. 1711–1719, Jan. 2005.

[34] S. B. Kim and E. G. Njoku, "Soil moisture retrieval using data cube representation of radar scattering," *Piers Online*, vol. 6, no. 6, pp. 504–508, 2010.

[35] A. Balenzano, F. Mattia, G. Satalino, and M. W. J. Davidson, "Dense temporal series of C- and L-band SAR data for soil moisture retrieval

over agricultural crops," *IEEE J. Sel. Topics Appl. Earth Observ. Remote Sens.*, vol. 4, no. 2, pp. 439–450, Jun. 2010.
[36] Y. Kim and J. J. van Zyl, "A time-series approach to estimate soil moisture using polarimetric radar data," *IEEE Trans. Geosci. Remoto Sens.*, vol. 47, no. 8, pp. 2519–2527, Aug. 2009.
[37] S. Yueh, S. Dinardo, S. Chan, E. Njoku, T. Jackson, and R. Bindlish, "Passive and active L-band system and observations during the 2007 CLASIC campaign," in *Proc. Int. Geosci. Remote Sens. Symp.*, 2008, p. II-244.
[38] A. Colliander, S. Chan, S.-B. Kim, N. Das, S. Yueh, M. Cosh, R. Bindlish, T. Jackson, and E. Njoku, "Long term analysis of PALS soil moisture campaign measurements for global soil moisture algorithm development," *Remote Sens. Environ.*, vol. 121, no. 0, pp. 309–322, Jun. 2012.
[39] R. Magagi, A. A. Berg, K. Goita, S. Belair, T. J. Jackson, B. Toth, A. Walker, H. McNairn, P. E. O'Neill, M. Moghaddam, I. Gherboudj, A. Colliander, M. H. Cosh, M. Burgin, J. B. Fisher, S.-B. Kim, I. Mladenova, N. Djamai, L.-P. B. Rousseau, J. Belanger, J. Shang, and A. Merzouki, "Canadian experiment for soil moisture in 2010 (CanEx-SM10): Overview and preliminary results," *IEEE Trans. Geosci. Remote Sens.*, vol. 51, no. 1, pp. 347–363, Jan. 2013.
[40] A. B. Smith, J. P. Walker, A. W. Western, R. I. Young, K. M. Ellett, R. C. Pipunic, R. B. Grayson, L. Siriwardena, S. Chiew, and H. Richter, "The murrumbidgee soil moisture monitoring network data set," *Water Resour. Res.*, vol. 48, no. 7, Jul. 2012.
[41] S. Peischl, J. P. Walker, C. Rüdiger, N. Ye, Y. H. Kerr, E. Kim, R. Bandara, and M. Allahmoradi, "The AACES field experiments: SMOS calibration and validation across the Murrumbidgee River catchment," *Hydrol. Earth Syst. Sci.*, vol. 9, no. 3, pp. 2763–2795, Mar. 2012.
[42] D. Gray, R. Yang, H. Yardley, R. Panciera, J. Walker, J. Hacker, A. McGrath, B. Bates, and N. Stacy, "PLIS: An airborne polarimetric L-band interferometric synthetic aperture radar," in *Proc. APSAR*, 2012, pp. 1–4.
[43] Y. Okada, T. Hamasaki, M. Tsuji, M. Iwamoto, K. Hariu, Y. Kankaku, S. Suzuki, and Y. Osawa, "Hardware performance of L-band SAR system onboard ALOS-2," in *Proc. IGARSS*, 2011, pp. 894–897.
[44] O. Merlin, J. Walker, R. Panciera, R. Young, J. D. Kalma, and E. J. Kim, "Soil moisture measurement in heterogeneous terrain," in *Proc. Int. Congr. MODSIM*, Dec. 2007, pp. 2604–2610.
[45] R. Panciera, "Effect of land surface heterogeneity on satellite near-surface soil moisture observations," Civil Environ. Eng., Univ. Melbourne, Melbourne, VIC, Australia, 2009.
[46] M. Shimada, O. Isoguchi, T. Tadono, and K. Isono, "PALSAR radiometric and geometric calibration," *IEEE Trans. Geosci. Remote Sens.*, vol. 47, no. 12, pp. 3915–3932, Dec. 2009.

Rocco Panciera received the M.S. degree in environmental engineering from the University of Trento, Trento, Italy, in 2003, and the Ph.D. degree in environmental engineering from the University of Melbourne, Melbourne, Vic., Australia, in 2009, with a thesis on the effect of land surface heterogeneity on the accuracy of spaceborne soil moisture retrieval using passive microwave techniques.

He worked at the University of Melbourne as a Research Fellow within the Soil Moisture Active Passive (SMAPEx) project for algorithm development for NASA's SMAP mission. In this role, he conducted two large scale field experiments in South-Eastern Australia including airborne active and passive microwave sensors. From January 2011, he has been based at the Cooperative Research Centre for Spatial Information (CRC-SI), Melbourne, Australia, where he is employed under the prestigious Superscience Fellowship from the Australian Research Council (ARC). In this role, he has been working on techniques to estimate fine-resolution soil moisture by use of L-band and X-band synthetic aperture radar (SAR) measurements. He has also been investigating the use of Light Detection and Ranging (LiDAR) techniques for fine-resolution retrieval of surface roughness characteristics in agricultural areas. His current field of interest is the retrieval of soil moisture from airborne and spaceborne SAR observations.

Jeffrey P. Walker received the bachelor's degrees in civil engineering and in surveying (with honors and university medal) and the Ph.D. degree in water resources engineering from the University of Newcastle, Australia, in 1995 and 1999, respectively. Ph.D. thesis was among the early pioneering research on estimation of root-zone soil moisture from assimilation of remotely sensed surface soil moisture observations.

In 1999, he joined NASA Goddard Space Flight Centre to implement his soil moisture work globally. In 2001, he moved to the Department of Civil and Environmental Engineering at the University of Melbourne as Lecturer, where he continued his soil moisture work, including development of the only Australian airborne capability for simulating new satellite missions for soil moisture. In 2010, he was appointed as Professor in the Department of Civil Engineering at Monash University, where he is continuing this research. He is contributing to soil moisture satellite missions at NASA, ESA, and JAXA as a Science Definition Team member for the Soil Moisture Active Passive (SMAP) mission and Cal/val Team member for the Soil Moisture and Ocean Salinity (SMOS) and Global Change Observation Mission—Water (GCOM-W), respectively.

Thomas J. Jackson (F'02) received the Ph.D. degree from the University of Maryland, College Park, MD, in 1976. His research involves the application and development of remote sensing technology in hydrology and agriculture, primarily microwave measurement of soil moisture. He is or has been a member of the science and validation teams of the Aqua, ADEOS-II, Radarsat, Oceansat-1, Envisat, ALOS, SMOS, Aquarius, GCOM-W, and SMAP remote sensing satellites. Currently, he is a research hydrologist with the U. S. Department of Agriculture, Agricultural Research Service, Hydrology and Remote Sensing Lab.

He is a Fellow of the Society of Photo-Optical Instrumentation Engineers, the American Meteorological Society, and the American Geophysical Union. In 2003, he received the William T. Pecora Award (NASA and Department of Interior) for outstanding contributions toward understanding the earth by means of remote sensing and the AGU Hydrologic Sciences Award for outstanding contributions to the science of hydrology. He received the IEEE Geoscience and Remote Sensing Society Distinguished Achievement Award in 2011.

Douglas A. Gray received the Ph.D. degree from the University of Adelaide, Adelaide, SA, Australia, in 1973. He spent 20 years with the Defence Science and Technology Organisation applying signal processing to sonar and electronic warfare and leading various research and development programs.

He is the Professor of Electrical Engineering at the Adelaide University and Director of the University of Adelaide Radar Research Centre. His current radar research interests are in MIMO radar, distributed radar networks for monitoring weather and synthetic aperture radar for surveillance and environmental monitoring.

Mihai A. Tanase received the engineering diploma in forestry from Stefan cel Mare University, Suceava, Romania, in 1999; the diploma in economy from the Bucharest Academy of Economic Studies, Bucharest, Romania, in 2004; the M.Sc. degree in environmental management from the International Centre for Advanced Mediterranean Agronomic Studies in Paris, France, in 2007; and the Ph.D. degree in geography from the University of Zaragoza, Zaragoza, Spain, in 2010.

Since 2011, he holds a postdoctoral position at the University of Melbourne through the ARC Super Science Fellowship program. He is a Principal Investigator for ESA ERS and DLR TerraSAR-X projects and participated in the K&C Initiative as a Co-Investigator. He is interested in the use of remote sensing for vegetation characterization. His current activity is focused on SAR, InSAR and PolSAR data for fire severity estimation, vegetation recovery monitoring and the retrieval of bio-geophysical parameters of forests and agricultural crops.

Dr. Tanase was the recipient of the IEEE GRSS IGARSS Symposium Interactive Prize Paper Award in 2010.

Dongryeol Ryu received the B.S. and M.S. degrees in geology from Seoul National University, Seoul, Korea, in 1997 and 2000, respectively, and the Ph.D. degree in earth system science from the University of California, Irvine, CA, in 2006.

Currently, he is a senior lecturer in the Department of Infrastructure Engineering, University of Melbourne, Melbourne, Vic., Australia. His specialization is hydrology with particular emphasis on remote sensing of land surface variables such as soil moisture and vegetation characteristics, their spatial and temporal variability, and hydrologic application of the remotely sensed land surface properties.

Dr. Ryu is a member of the IEEE Geoscience and Remote Sensing Society, the American Geophysical Union, and the Engineers Australia.

Alessandra Monerris received the B.E. degree in telecommunication from the Universitat Politècnica de València, València, Spain, and the Ph.D. degree in electrical engineering from the Universitat Politècnica de Catalunya, Barcelona, Spain. In 2006, she was a Visiting Ph.D. Student at the Universita Tor Vergata, Rome, Italy. From 2007 to 2011, she was Executive Director at the Soil Moisture and Ocean Salinity Expert Centre in Barcelona (SMOS-BEC). Currentl, she is a Research Fellow at the Department of Civil Engineering from Monash University. She has been involved in many field experiments sponsored as part of the preparatory activities for ESA's SMOS mission, and coordinated the Third Soil Moisture Active Passive Experiment (SMAPEx-3) in preparation of NASA's SMAP mission launch. She is also managing the OzNet soil moisture monitoring network in the Murrumbidgee River Catchment, Australia. Her research interests deal with the estimation of soil moisture and vegetation parameters from L-band passive observations, cosmic-ray probes and Global Navigation Satellite Systems Reflectometry (GNSS-R).

Heath Yardley, photograph and biography not available at the time of publication.

Christoph Rüdiger (M'10) received the B.E. degree in civil engineering from the University of Applied Sciences, Wiesbaden, Germany, in 2002, and the Ph.D. degree in environmental engineering from the University of Melbourne, Melbourne, Vic., Australia, in 2007, studying the potential to assimilate streamflow data into land surface models for soil moisture prediction. His undergraduate thesis covered the topic of groundwater and contaminant flow around future buildings.

In 2007, he joined the Centre National de Recherches Météorologiques (CNRM) at Météo France in Toulouse to work on the preparation of surface soil moisture and LAI data assimilation into the French land surface model ISBA. During this period, he also worked on the validation of different passive and active microwave satellite products over France, with a particular focus on ESA's SMOS. Since his return to Australia in July 2008, he has coordinated and led a number of cal/val campaigns for the Australian land validation segment of SMOS mission in the Australian arid zone and the Murrumbidgee River catchment. In addition to this, he continues to work on land surface data assimilation and also participates in the Australian cal/val segments for NASA's SMAP and Aquarius. His current fields of interest are in the remote sensing of vegetation dynamics and landscape water content. He is currently a lecturer at Monash University in Melbourne, Australia.

Xiaoling Wu, photograph and biography not available at the time of publication.

Ying Gao, photograph and biography not available at the time of publication.

Jörg M. Hacker received the Dr. rer. nat. degree in atmospheric sciences from the Meteorological Institute, University of Bonn, Bonn, Germany, in 1980, where he held the position of Research Fellow until 1982.

In 1982, he took up a position as a Post-Doctoral Fellow at the Flinders University of South Australia in Adelaide/South Australia. He then built up Australia's National Research Aircraft Facility ARA—Airborne Research Australia, which today is Australia's only National Facility engaged in using and operating aircraft for atmospheric and environmental research. Today, he is ARA's Director and Chief Scientist and also holds the position of Associate Professor within Flinders University. His research work spans a wide area, with special emphasis on the atmospheric boundary layer and the development of innovative instrumentation and measurement strategies using airborne platforms. He was coauthor in more than 80 publications in internationally refereed journals and more than 150 Conference Papers. He pioneered the concept of using cost-efficient small aircraft for atmospheric research, including the research described in the current paper. For his international science activities, in 1994 together with colleagues Professor Helmut Kraus (University of Bonn) and Professor Peter Schwerdtfeger (Flinders University), JM Hacker received the prestigious Max Planck Prize, awarded jointly by the German Alexander von Humboldt Foundation and the Max Planck Society. Together with H.W. Grosse, he holds the World Record for flying a self-launching glider over a 500-km triangle at an average speed of 172 km/h.